Development of ionic liquids for the use of conducting-bridge random access memory

July, 2016

Akinori Harada

The Graduate School of
Engineering
(Doctor Course)
TOTTORI UNIVERSITY

Tottori University

Contents

Chapter 4. Copper Ion Containing Ionic Liquids Provides Improved Endurance and Switching Voltage Distributions of CB-RAM

Chapter 5. Influence of Ionic liquids physicochemical properties for the Performance Improvements of CB-RAM.

Chapter 6. Summery ·················· 45

Chapter 7. Ionic liquid syntheses ·················· 46

Chapter 8. Measurement methods for physicochemical properties of ILs ······· 61

Chapter 9. Physicochemical properties of ILs ·················· 62

Chapter 10. References ·················· 64

Chapter 11. Publications ·················· 68

Acknowledgment ·················· 71

Abbreviation

Abbre-viation	Meaning	Abbre-viation	Meaning
IL	ionic liquid	CB-RAM	Conducting-Bridge Random Access Memory
V_{form}	forming voltage		
V_{set}	set voltage	V_{reset}	reset voltage
I_{form}	forming current	I_{set}	set current
I_{reset}	reset current	I_{comp}	current compliance
R_H	high resistance	R_L	low resistance
[emim]	1-ethyl-3-methylimidazolium	[bmim]	1-butyl-3-methylimidazolium
[hmim]	1-(n-hexyl)-3-methylimidazolium	[omim]	1-methyl-3-octyllimidazolium
[bdmim]	1-butyl-2,3-dimethylimidazolium	[MEmim]	1-(2-methoxyethyl)-3-methylimidazolium
[bmtr]	1-butyl-3-methyl-1,2,3-triazolium	[N$_{1224}$]	N-butyl-N,N-diethyl-N-methylammonium
[PP$_{14}$]	1-butyl-1-methypiperidinium	[Py$_4$]	1-butylpyridinium
[Tf$_2$N]	bis(trifluoromethane-sulfonyl)amide	[FSA]	bis(fluorosulfonyl)amide
[BF$_4$]	tetrafluoroborate	[PF$_6$]	hexafluorophosphate
[DCA]	dicyanamide	[TfO]	trifluoromethanesulfonate
[MeSO$_4$]	methyl sulfate	[Me$_2$PO$_4$]	dimethyl phosphate

Chapter 1. Introduction

1-1. Ionic Liquid (IL)
1-1-1. IL

ILs are special salts that have low melting points at around room temperature, and recently, have attracted strong interest because of their many attractive characteristics of low-volatility, less flammable nature, high ion conductivity, and a wide potential window.[1–3] Most ILs consist of organic moieties (Figures 1-1, 1-2), thus their physicochemical properties are tunable by changing the structure. Because of their attractive chemical properties, IL application studies for electric devices are currently showing significant interest.[1,2,4–6]
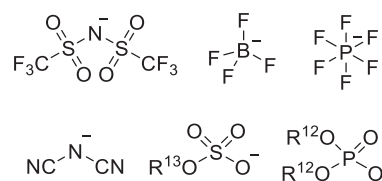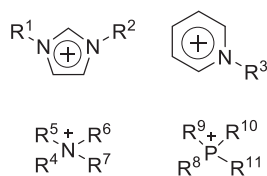

Figure 1-1. Typical cation structure of IL   **Figure 1-2.** Typical anion structure of IL

1-1-2. Attractive physicochemical properties of ILs
Ionic conductivity

The ionic conductivity of a solvent is important for use in electrochemical devices. ILs usually have a higher ionic conductivity than molecular solvents, for example, the ionic conductivity of [emim][Tf$_2$N] is 9.2 mS/cm at 25 °C in contrast to that of methanol of 1.5×10^{-7} mS/cm at the same temperature.[7] ILs, which have a high ionic conductivity, can transport metal ions with low an energy which is important for electrochemical devices such as batteries, electric double layer capacitors and solar cells.[1,8–13] The trend in ionic conductivity with respect to the cation type follows the order: imidazolium > ammonium > pyridinium.[14] The conductivity and viscosity of the ILs are often combined into what is termed Walden's rule: (ionic conductivity)×(viscosity) = constant.[14] The ILs with a low viscosity has a high ionic conductivity. Hagiwara and his co-workers developed excellent highly ionic conductive fluorohydrogenate ILs, such as [emim][(HF)$_{2.3}$F], which has an ionic conductivity of 100 mS/cm[15,16]

Electrochemical window

The key factor of a solvent for electrochemical studies is the electrochemical stability of the solvent, i.e., the electrochemical window.[1,14] This property suggests the range of voltages over which the solvent is electrochemically inert. This electrochemical window depends on the oxidative and

reductive stability of the solvent. For ILs, the electrochemical window primarily depends on the resistance of the cation to reduction and the resistance of the anion to oxidation. In most cases, the ILs have wider electrochemical windows than water. Thus, the ILs can be used for electrochemical devices with a higher voltage range than the water system. The trend in the electrochemical stabilities of the IL cation types is: ammonium > imidazolium > pyridinium.[14] The anion stabilities towards oxidation appear to follow the order: triflyl ions ([Tf_2N], [FSA]) > fluorinated ions ([BF_4], [PF_6]) > halides (Cl, Br, I).[14]

1-2. Memory device
1-2-1. Memory device

The memory is an electric device memorizes the obtained information, and the importance of memory devices has considerably increased in recent years. The amount of information is significantly increasing, thus, studies about enhancing the memory capacity are now investigated all over the world.

1-2-2. Problems of currently used memories

SRAM (static random access memory), DRAM (dynamic random access memory) and the NAND-type flash memory are currently used in PCs, and their capacities are growing. However, serious problems have become apparent.

The first problem is the necessity for the combined use of several types of memories. As mentioned above, at least 3 types of memories are used in PCs because they have strong and weak points. For example, the SRAM and DRAM can quickly write and read but they cannot memorize a significant amount of information. Furthermore, they cannot store information without a power supply, i.e., a volatile nature. On the other hand, the NAND-type flash memory has a relatively high capacity and non-volatile nature, but its operating speed is slow. Thus, a universal memory, which has a high information density, high speed and non-volatile nature is desired. The second problem is the capacity growth limit of the NAND-type flash memory. NAND-type flash memories hold a prominent position among memory devices, and they memorize information by storing an electrical charge in their gate. To achieve a high capacity memory, reductions in the cell size becomes essential. However, in the case of the NAND-type flash memory, a very small cell structure caused serious data errors by the infection of electron in the gate to adjacent cell. The development of a new memory architecture is now desired.[17]

1-2-3. Conducting-bridge random access memory (CB-RAM)

The resistive switching memory (ReRAM) and magnetic random access memory (MRAM) have gained growing interest as next-generation non-volatile memories.[18] The CB-RAM is a kind of Re-RAM and is a promising candidate for the next-generation memory.[18–21] The CB-RAM displays very attractive memory properties, such as a high speed, high resistance ratio, and high density, based on its simple device architecture as shown in Figure 1-3 and Table 1-1.
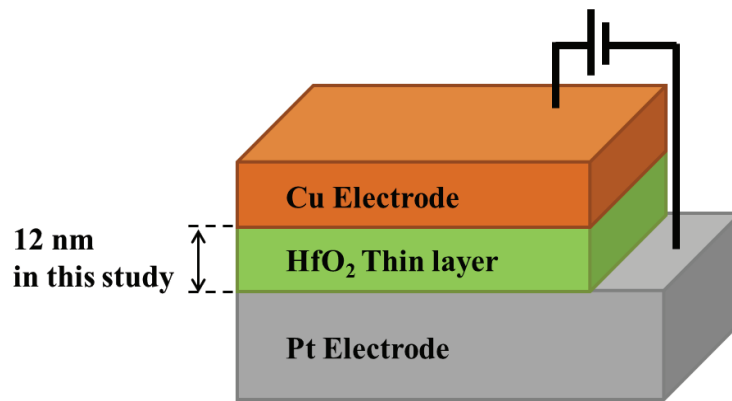

Figure 1-3. Simple memory architecture of CB-RAM

Table 1-1. Best properties of DRAM, NAND Flash and CB-RAM.

	DRAM	NAND-type Flash	CB-RAM
Cell size	6～8 F^2	2～20 F^2	2～8 F^2
Write/read speed	5 ns	10 ms	< 10 ns
Data retention time	< 100ms	10 years	10 years

1-2-4. Proposed switching mechanism of CB-RAM

Although details of the resistive change mechanisms in solid electrolyte switching devices are not yet fully understood, one of the most plausible mechanisms is the formation and annihilation of filamentous metal conduction paths in the solid electrolyte as illustrated in Figure 1-4, the resistive switching phenomenon is therefore caused by a conductive bridge which is created by the reduction and deposition of metal ions which are eluted from the positively biased active electrode into a metal oxide (1: Forming step). Next, the conductive bridge ruptures by applying a negative bias to the active electrode, producing a highly resistance state (2: Reset step). The conductive bridge is then re-

produced by applying a positive bias again, resulting in a low resistance state (3: Set step). The reset and set steps are alternately repeated by applying negative and positive biases, respectively.[18,22–25] Although the performance of the Cu/HfO$_2$/Pt CB-RAM is already superior to the present non-volatile memories in terms of a lower operating voltage and higher memory capacity, further development of the methodology to reduce the switching voltages is needed in order to realize the next generation CB-RAM.
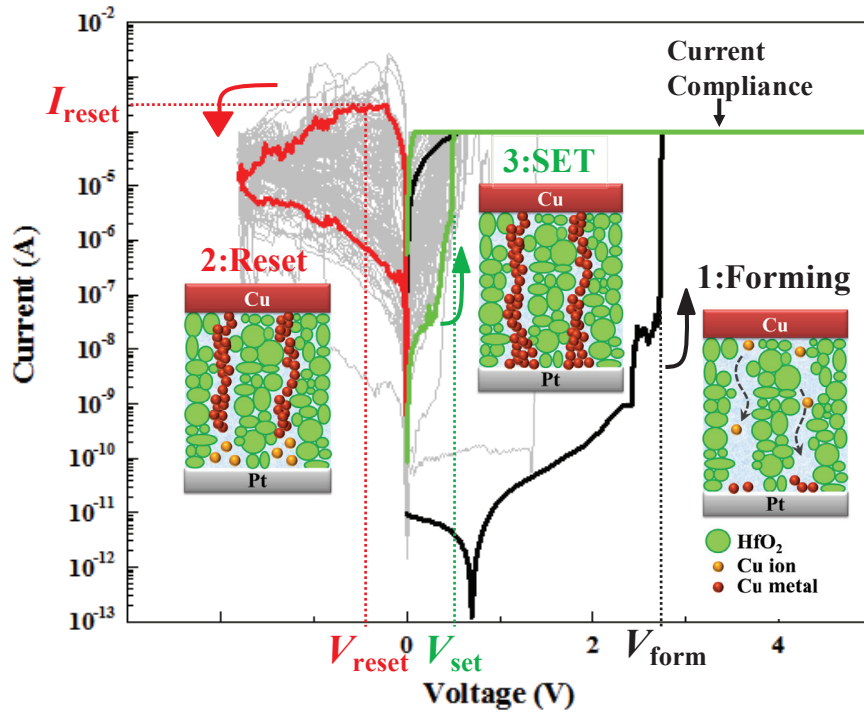

Figure 1-4. Typical *I-V* curve and proposal switching processes in the Cu/HfO$_2$/Pt CB-RAM

1-2-5. The role of water in the fine pore space of HfO$_2$ layer

Tsuruoka and coworkers reported a water addition effect on SiO$_2$ and Ta$_2$O$_5$ regarding the switching characteristics of the Cu/MO/Pt cell (MO = SiO$_2$ or Ta$_2$O$_5$); the ambient moisture that condensed in the grain boundary of the MO film influenced the migration and/or redox of the copper (Cu) atoms and thus affected the resistive switching voltages (Figure 1-5).[25,26] We also demonstrated that supplying water to the HfO$_2$ film in the Cu/HfO$_2$/Pt cell significantly reduced the switching voltage as shown in Figure 1-6.[27,28] The reduction of the operating voltages by supplying water to HfO$_2$ film of the Cu/HfO$_2$/Pt cell structure was then achieved.
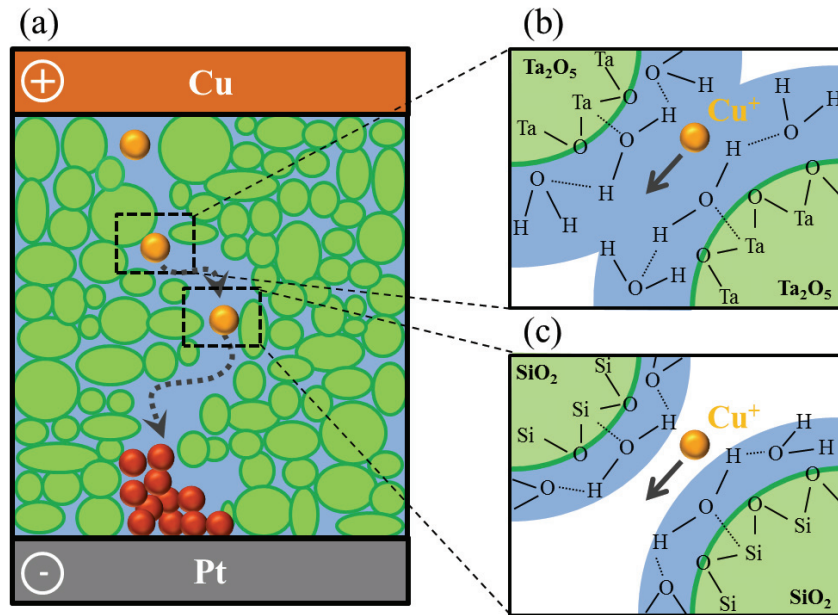
Figure 1-5. Potential mechanism for the moisture effects on the ionization of Cu and the migration of Cu ions in an oxide-based atomic switch (a). Schematics (b) and (c) illustrate the bonding states of the residual water molecules at the grain boundaries in the Ta_2O_5 and SiO_2 layers, respectively. [25]
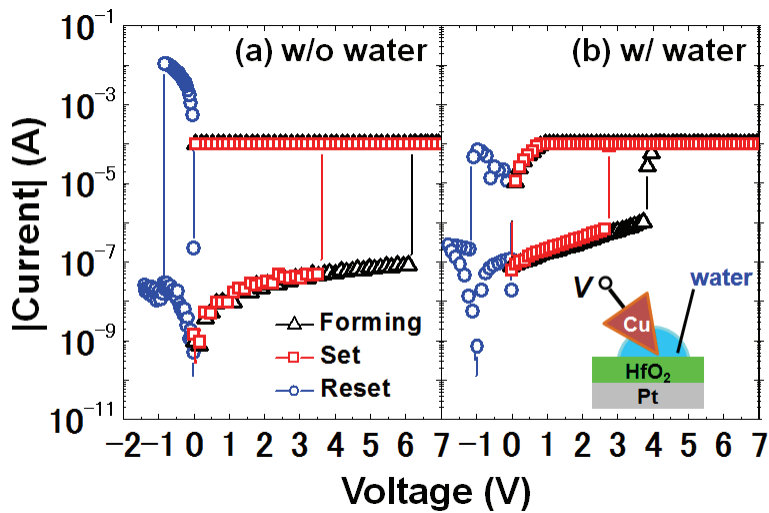

Figure 1-6. Typical *I-V* characteristics of (a) water-non-supplied and (b) water-supplied $Cu/HfO_2/Pt$ structures in the atmosphere.[28]

1-3. The objective of this thesis

The present operating voltage and cycling endurance of the CB-RAM are, however, still insufficient for practical use, therefore, development of an efficient means to reduce their operating voltage and high cycling endurance in the resistive switching process has been significantly desired. As already described , we demonstrated that supplying water to the HfO_2 film in a $Cu/HfO_2/Pt$ cell significantly reduced the switching voltage.[28] However, due to the volatility and electrochemical instability of water, the HfO_2 film decomposed during the switching cycles. Water is obviously unsuitable for use in memory devices that require a high reliability; it is necessary to find an alternative additive to the water. We turned our attention to ILs to solve this problem. ILs have attracted strong interest because of their already described characteristics. We then envisioned that the ILs would act as an alternative to water and improve the CB-RAM properties by accelerating the migration rate of the Cu ions.

Chapter 2. Evaluation method of IL's effect on the CB-RAM performance

2-1. Cell structure

2-1-1. Cell structure for measurements

Because of the simplicity of the experiments, we put a drop of the IL on the surface of HfO_2. The Cu-probe/HfO_2/Pt structure was then created by contacting the surface of the HfO_2 film with a Cu-probe, as shown in Figure 2-1.
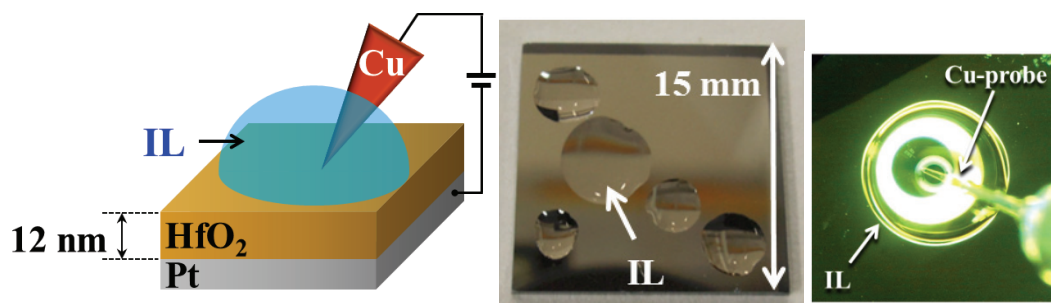
Figure 2-1. The Cu-probe/HfO_2/Pt structure for *I-V* characteristic measurements
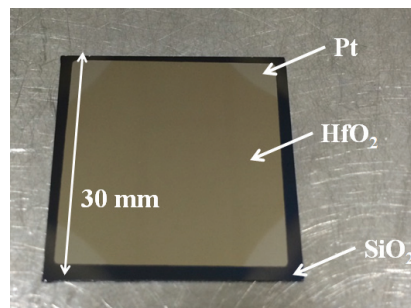
Figure 2-2. Cell for *I-V* characteristics measurements

2-1-2. Preparation of Cu-probe/HfO_2/Pt cell

A HfO_2 layer with a thickness of 12 nm was deposited on a Pt (100 nm)/Ti (20 nm)/SiO_2 (100 nm)/Si (650 μm) substrate in a mixed gas of Ar and O_2 (Ar : O_2 = 3.8 : 1.5 Pa) using the RF reactive sputtering method. The apparatus for the sputtering is shown in Figure 2-3. The total gas pressure, RF power and substrate temperature were maintained at 5.3 Pa, 100 W and 300 °C, respectively (Figure 2-4).

Figure 2-3. Picture of the sputtering apparatus
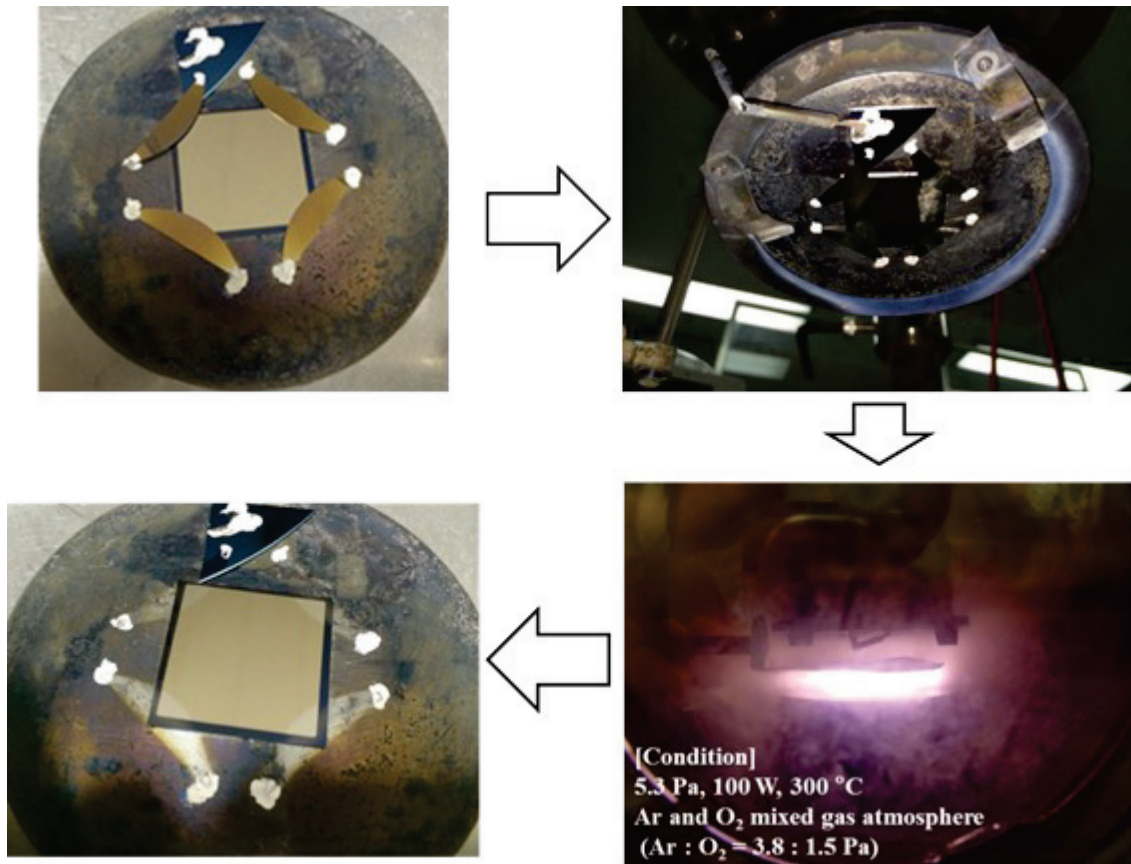
Figure 2-4. Picture of sputtering process for HfO$_2$ layer construction

2-1-3. Thickness of HfO₂ layer

The effect of HfO_2 layer thickness on the operating voltages (V_{form} and V_{set}) was investigated. The operating voltages were reduced according to reducing the thickness as shown in Figure 2-5. The thinnest condition of a 6 nm HfO_2 thickness gave the lowest operating voltages. This result might be caused by the shortening of Cu 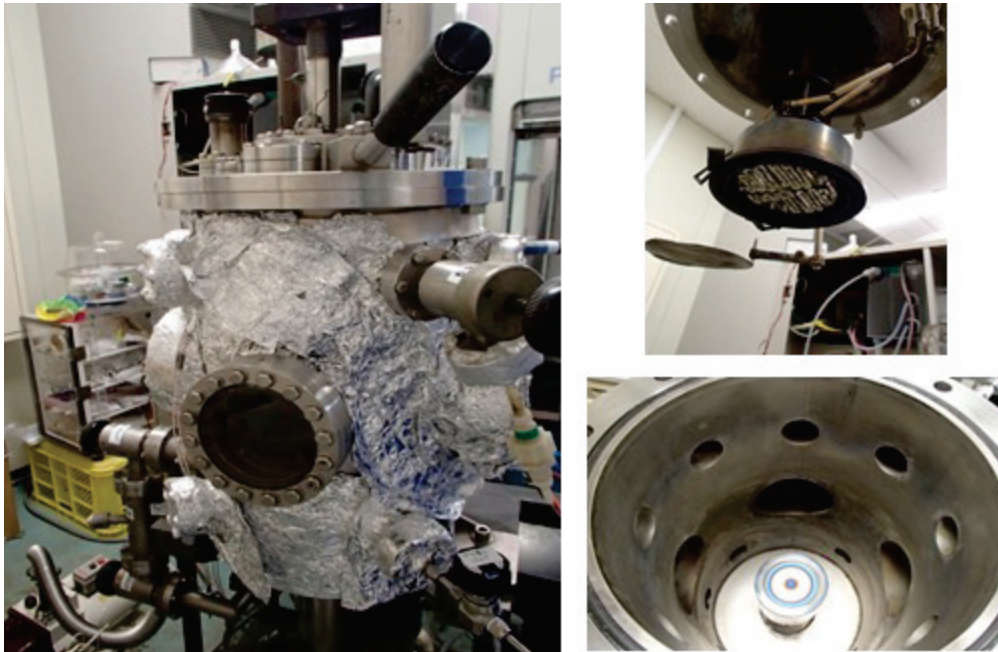ion migration path way.   However, for the 6 nm condition, the operating voltages widely ranged (Figure 2-6) and a good reproducibility was not obtained. In contrast, better reproducibility was obtained under the 12 nm condition. To determine the reason of these results, we analyzed the HfO_2 thin film with 6, 12 and 60 nm thickness by x-ray diffraction (XRD). The result shown in Figure 2-7 suggested that the film was amorphous for the 6 nm thickness. It is postulated that the fine pore structure was not uniform and caused the bad reproducibility. However, the exact reason is yet not fully understood.
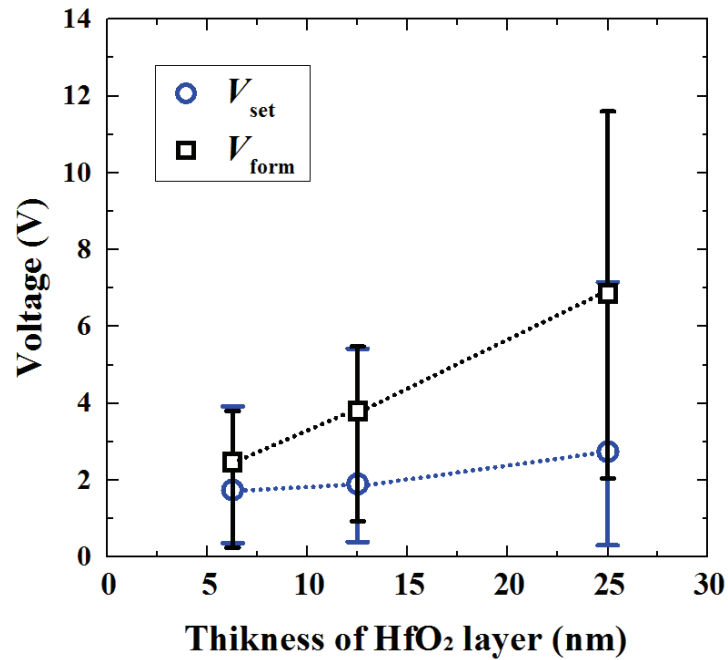
Figure 2-5. Thickness of HfO₂ layer dependence on the operating voltages
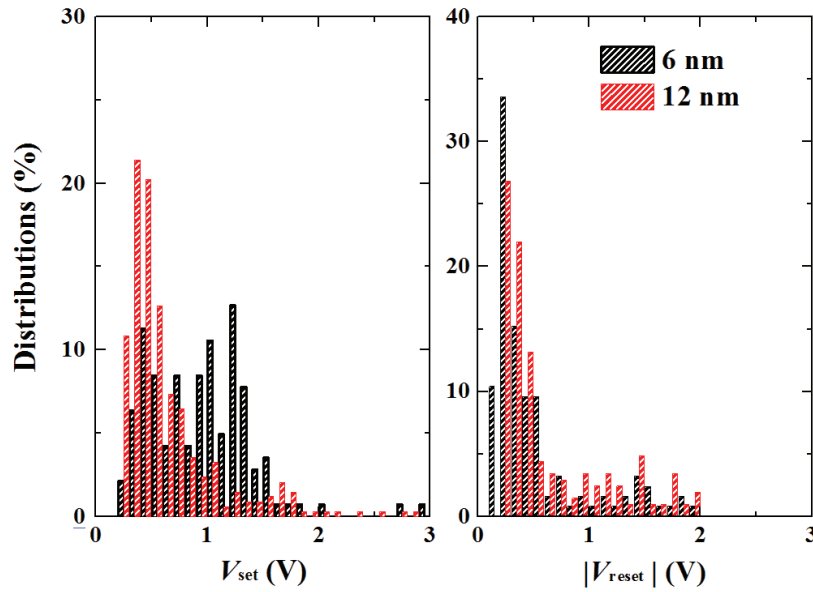
Figure 2-6. Distributions of operating voltages when the HfO$_2$ thickness was 6 nm or 12 nm.
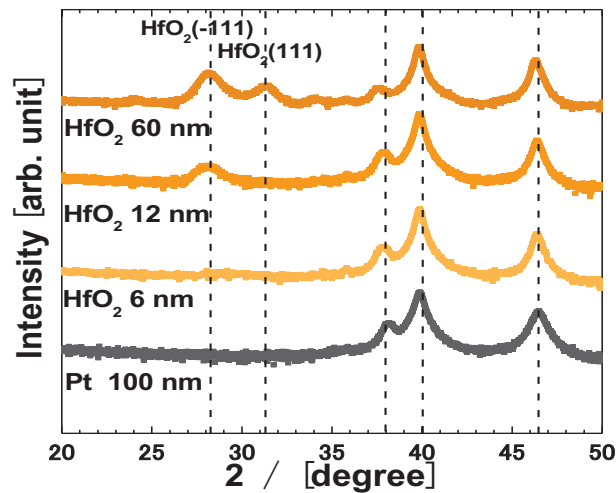
Figure 2-7. XRD results of HfO$_2$ layer with 6, 12 or 60 nm thickness

2-1-4. The fine pore spaces in the HfO$_2$ layer

It is known that the HfO$_2$, which is created by a sputtering method, has fine pore spaces (Figure 2-8) following the axiom of the structure zone model.[28,29] According to the reported side view TEM image of the HfO$_2$, the size of each HfO$_2$ pore was estimated to be ca. 2~5 nm and the wall width between the pores was around 10 nm (Figure 2-8).[28] Therefore, the necessary volume of the IL which could completely fill the inside of the HfO$_2$ film was estimated to be less than 9.2×10^{-5} μL

when we used a film which is 1.0 square centimeter and 12 nm thick. Thus, a drop of IL (ca. 0.1 μL) is enough to fill the fine pore spaces of the HfO$_2$ film.
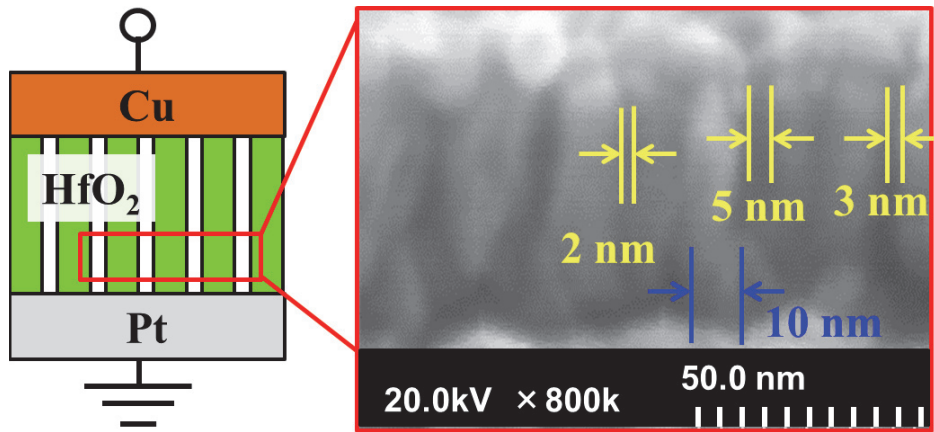
Figure 2-8. TEM image of HfO$_2$ layer[28]

2-1-5. *Method of preparing Cu-probe*

The Cu-probe was made by sputtering metallic copper of which the purity was over 99.99% on a tungsten needle with the radius of 10 μm. The Cu-probe is shown in Figure 2-9.
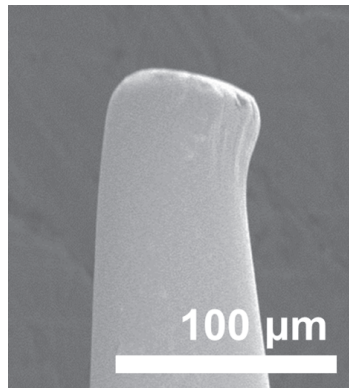
Figure 2-9. Picture of the Cu-probe

2-2. Measuring method

The picture of the apparatus for the measurement is shown in Figure 2-10. A drop of IL (ca. 0.1 μL) was placed on the surface of the HfO_2 film and then the Cu-probe was brought into contact with the surface through the IL droplet as explained in section 2-2-1. The tungsten(W)-probe was in contact with the surface of the Pt as the ground. All the measurements were performed under flowing nitrogen to avoid water absorption into the ILs except for those in chapter 3. Only in chapter 3 were the measurements performed under ambient air conditions, because the experiments investigated the water effect on the operating voltages. The detailed parameters of measurements for the current-voltage (I-V) characteristics were described in the experimental sections of each chapter.
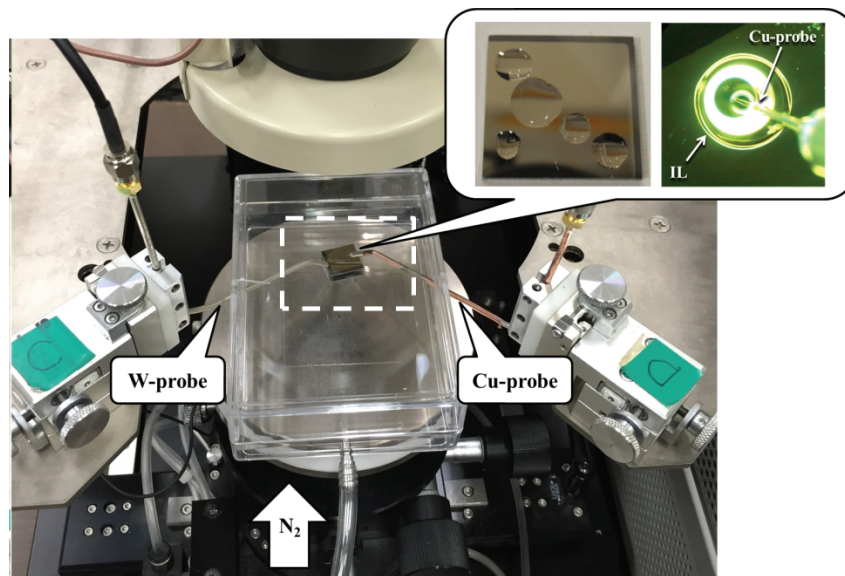
Figure 2-10. Apparatus for measuring

Chapter 3. Enhanced Stability of the HfO$_2$ Electrolyte and Reduced Working Voltage of a CB-RAM by an Ionic Liquid

3-1. The introduction and objective of this study

As described in Chapter 1, we envisioned that ILs would act as an alternative to water and improve the CB-RAM properties by accelerating the migration rate of Cu ions. Then, we investigated addition effects of IL for the switching characteristics of CB-RAM.

3-2. The additive effect of IL for operating voltages

We chose 1-butyl-3-methylimidazolium bis(trifluoromethanesulfonyl)amide ([bmim][Tf$_2$N]) as a model IL and evaluated the effect of supplying IL by the cumulative probabilities of the forming voltage (V_{form}), the set voltage (V_{set}) and the reset voltage (V_{reset}). Since ILs are generally hydrophilic and it is known that even "hydrophobic ILs" absorb ca. 1.0 wt% (10,000 ppm) of water under ambient air conditions,[30] we prepared samples of [bmim][Tf$_2$N] containing 5000 ppm of ultrapure water and investigated the effect on the performance of the CB-RAM by the cumulative probabilities of the Cu/HfO$_2$/Pt cell under three conditions, ultrapure water (H$_2$O), IL (which contains 5000 ppm of water) and blank conditions (Figure 3-1) (Typical *I-V* curve were showed in Figure 3-2, 3-3, 3-4). We evaluated the effect of supplying the IL by a V_{form} value at which the cumulative probability of Vform becomes 50%, $V_{form}^{50\%}$. Although we envisioned that supplying IL to the HfO$_2$ film might accelerate the ion migration rate and reduce the V_{form}, the lowest $V_{form}^{50\%}$ (0.75 V) was observed when H$_2$O was supplied (Figure 3-1-a). However, the reduction of $V_{form}^{50\%}$ (3.15 V) was indeed attained when IL was used as a solvent. The reduction rate of $V_{form}^{50\%}$ by supplying IL from $V_{form}^{50\%}$ of blank samples (4.30 V) is estimated to be 26 % (= (4.30 V - 3.15 V) / 4.30 V) and is significant, although not as much as the reduction rate by supplying water, 83 %.   On the other hand, V_{set} was reduced by IL from V_{set} of blank samples as effectively as by supplying H$_2$O (Figure 3-1-b). A V_{set} value at which the cumulative probability of V_{set} becomes 50%, $V_{set}^{50\%}$, for the blank, water- and IL-supplied samples are 0.83, 0.65 and 0.65 V, respectively. Therefore, $V_{set}^{50\%}$ was reduced by 22 % by supplying IL as well as water. This reduction rate of V_{set} is very significant because set switching is not a one-time process like a forming process, although the reduction rate of $V_{set}^{50\%}$ of 22 % is smaller than that of $V_{form}^{50\%}$ of 26 %. The reduction of V_{form} and V_{set} strongly suggests that the addition of polar solvents such as water and IL facilitates formation of a filament by the enhancement of electrochemical dissolution. It is noteworthy that the addition of IL is effective even in reducing V_{reset}, as shown in Figure 3-1-c. V_{reset} values at which the cumulative probability of V_{reset} becomes 50%, $V_{reset}^{50\%}$ were 0.60, 0.34, 0.50 V for blank, water, and IL-supplied samples, respectively. Therefore, it is suggested that not only the thermally-assisted diffusion of Cu atoms composing the Cu-filament

16

but also the electrochemical dissolution of the Cu-filament contribute to the occurrence of reset switching.
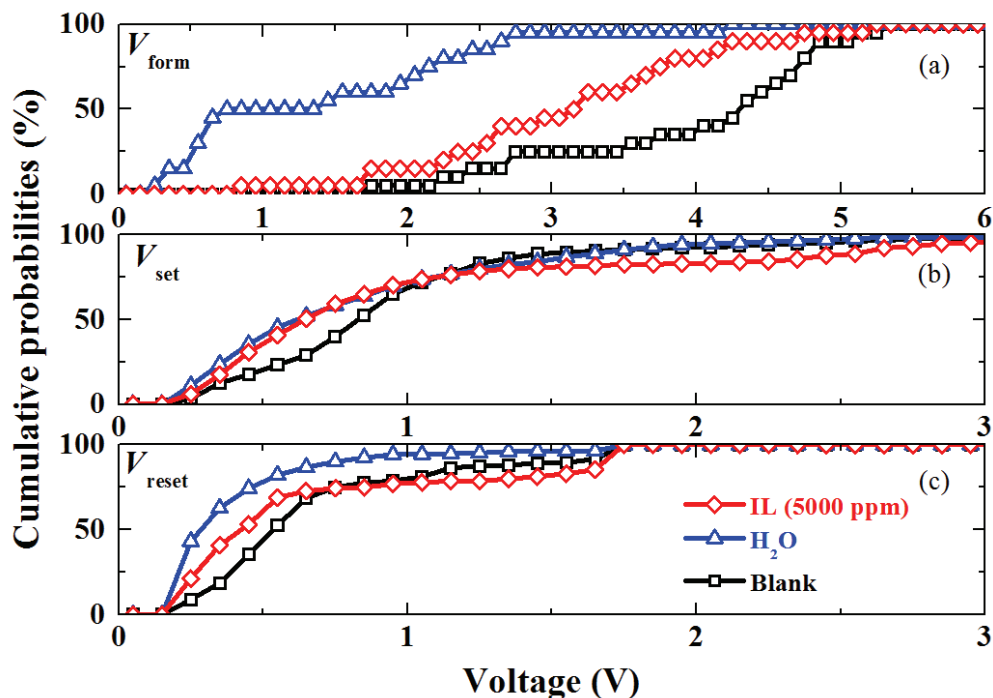
Figure 3-1. Cumulative probabilities of the $Cu/HfO_2/Pt$ measured in the presence of IL ([bmim][Tf$_2$N]) and H_2O. "Blank" indicates the results of a control experiment without any additive.

Table 3-1. Average values of V_{form}, V_{set} and V_{reset} measured in the presence of IL and H_2O.

	Blank	H$_2$O	IL
Additive	none	Ultra pure water	[bmim][Tf$_2$N]
V_{form} (average)	4.30 V	0.75 V	3.15 V
V_{set} (average)	0.83 V	0.65 V	0.65 V
V_{reset} (average)	0.60 V	0.34 V	0.50 V
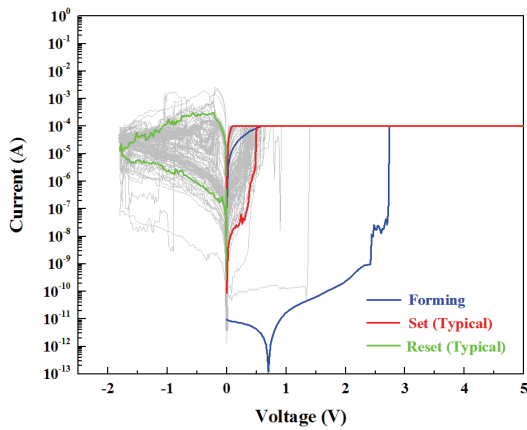
Figure 3-2. Typical *I-V* curve of CB-RAM with a control experiment without any additive in Figure 3-1.
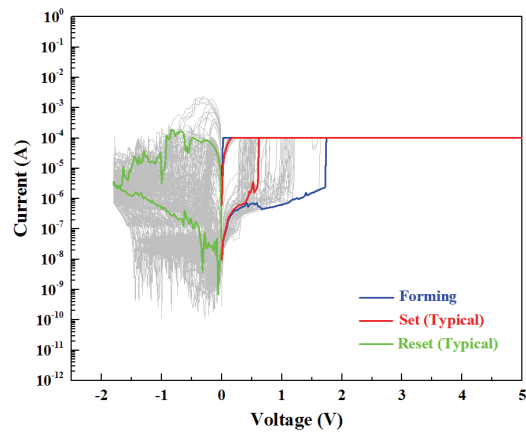
Figure 3-3. Typical *I-V* curve of CB-RAM with ultrapure water on the surface of HfO_2 film in Figure 3-1.

Figure 3-4. Typical *I-V* curve of CB-RAM with IL (water content 5,000ppm) on the surface of HfO_2 film in Figure 3-1.

3-3. The effect of water contaminated in IL for operating voltages

We next investigated the influence of water contaminated to IL. Then, we prepared three samples of the [bmim][Tf$_2$N], involving 100 ppm, 800 ppm, and 5,000 ppm (0.500 wt%) of ultrapure water and tested the effect of supplying these ILs on the performance of the CB-RAM by the cumulative probabilities of the Cu/HfO$_2$/Pt cell. The results of the comparative study are shown in Figure 3-5 (Typical *I-V* curve were showed in Figures 3-6, 3-7 and 3-8). The lowest V_{form} (2.45 V) was confirmed when the IL (800 ppm of water) was supplied to the HfO$_2$ film, and similar V_{form} voltages were observed for the cells with the ILs which contained 100 and 5,000 ppm of water, respectively. These results clearly indicate that the IL contributed to reduction of the working voltage of the CB-RAM, though a trace amount of water in the IL might play an important role in the performance. H$_2$O molecules in ILs are known to be electrostatically dissociate into protons and hydroxyls.[31,32]

Tappertzhofen and co-worker reported that the importance of water in switching behavior of CB-RAM. The formation of metallic cations proceeds in parallel to reduction of moisture, supplied by the ambient, and it suggested that necessity of a counter charge/reaction to keep the charge electro neutrality in cation-transporting thin films.[26] Yuan and coworkers applied IL containing 500 ppm of water to a thin film transistor (TFT) as a gate dielectric.[33] They reported that the dissociated H^+ and OH^- ions in the IL acted as inner Helmholtz layers and reduced the capacitor gap of an electric double layer capacitance (EDLC). In our case, the formation of inner Helmholtz layers might strengthen the electric field intensity at the Cu/HfO_2 and HfO_2/Pt interfaces and enhance the charge transfer at the interfaces, resulting in the reduction of working voltages.

Figure 3-5. Cumulative probabilities of the $Cu/HfO_2/Pt$ measured in the presence of IL samples with different water content.

Figure 3-6. Typical *I-V* curve of CB-RAM with IL (water content 100ppm) on the surface of HfO_2 film in Figure 3-5.

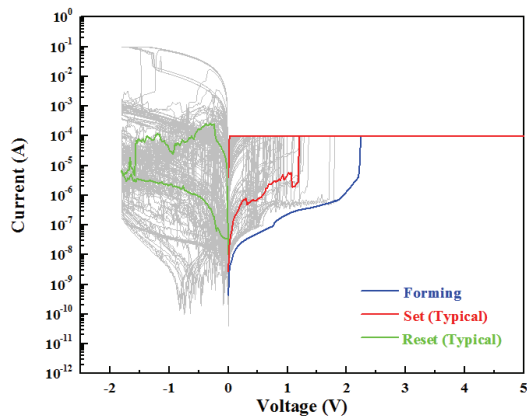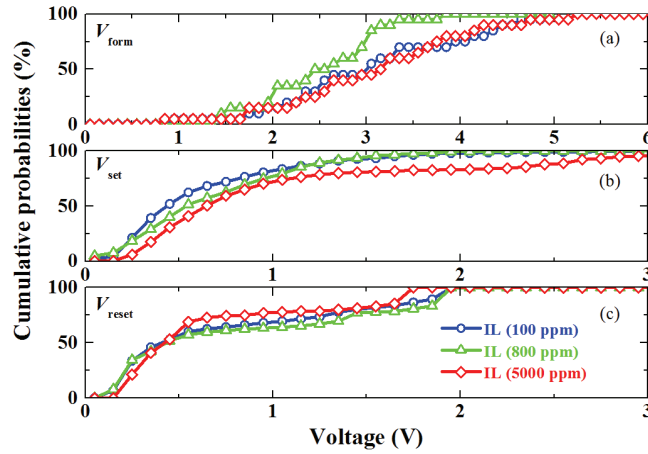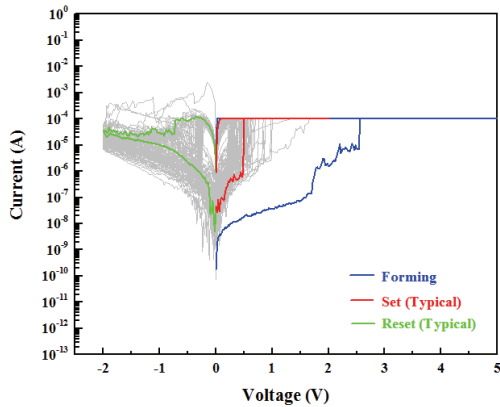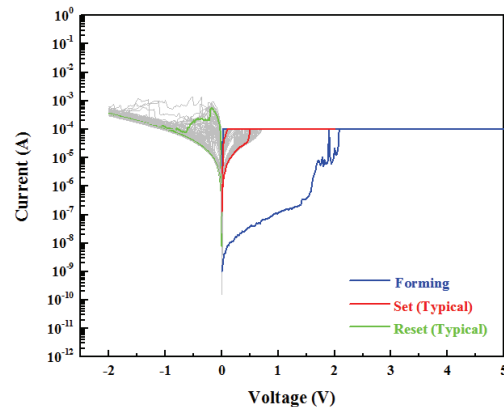**Figure 3-7.** Typical *I-V* curve of CB-RAM with IL (water content 800ppm) on the surface of HfO_2 film in Figure 3-5.
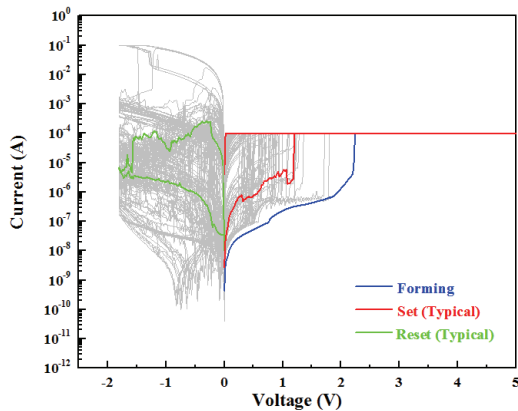
Figure 3-8. Typical *I-V* curve of CB-RAM with IL (water content 5,000ppm) on the surface of HfO_2 film in Figure 3-5.

3-4. The stress test

Although water can most effectively decrease switching voltages, the Vform value of water supplied samples at which the cumulative probability of V_{form} becomes 100% is 4.25 V. The electrolysis of water might take place at this voltage. Therefore, we conducted the voltage stress test using the Cu-probe/HfO_2/Pt cell, which is the same cell structure as used for the above measurements, in the presence of water or the IL as follows: a drop of ultrapure water was added to the surface of the HfO_2 film which was deposited on the Pt electrode, then the Cu-probe was brought into contact with the surface of the HfO_2 film. The voltage was ramped up from 0 to 10 V and then ramped down to 0 V in steps of 0.02 V intervals with 640 μs per plot. *I-V* characteristic of the voltage ramping profile (Figure 3-9-A) shows forming occurred at 4.0 V. Then the Cu-probe was removed, followed by the removal of water by washing with acetone and drying under air conditions, and the surface of HfO_2 film was observed (for details of this experiment was showed in Figure 3-9). As shown in Figure 3-9, decomposition of the HfO_2 film was, in fact, observed when water was supplied on the surface of the film (Figure 3-9-a); HfO_2 was assumed to be decomposed due to hydrogen- or oxygen-gas generated by the electrolysis of water. Since the Cu-probe and Pt electrode are short-circuited by conductive Cu-filament after the forming process, the film decomposition occurred at least below 4.0 V. This means that we cannot use water to practically improve performance of the present CB-RAM cell, even though it could contribute to reduction of the working voltage. On the other hand, no decomposition of the HfO_2 film was observed even when the voltage was ramped up to 15 V in the presence of the IL which contained 5,000 ppm of water, as can be seen in Figure 3-9-b. *I-V* characteristic of the voltage ramping profile (Figure 5-9-B) shows forming occurred at 9.2 V. This clearly indicates that the use of IL improves the stability of CB-RAM against voltage stress.

20

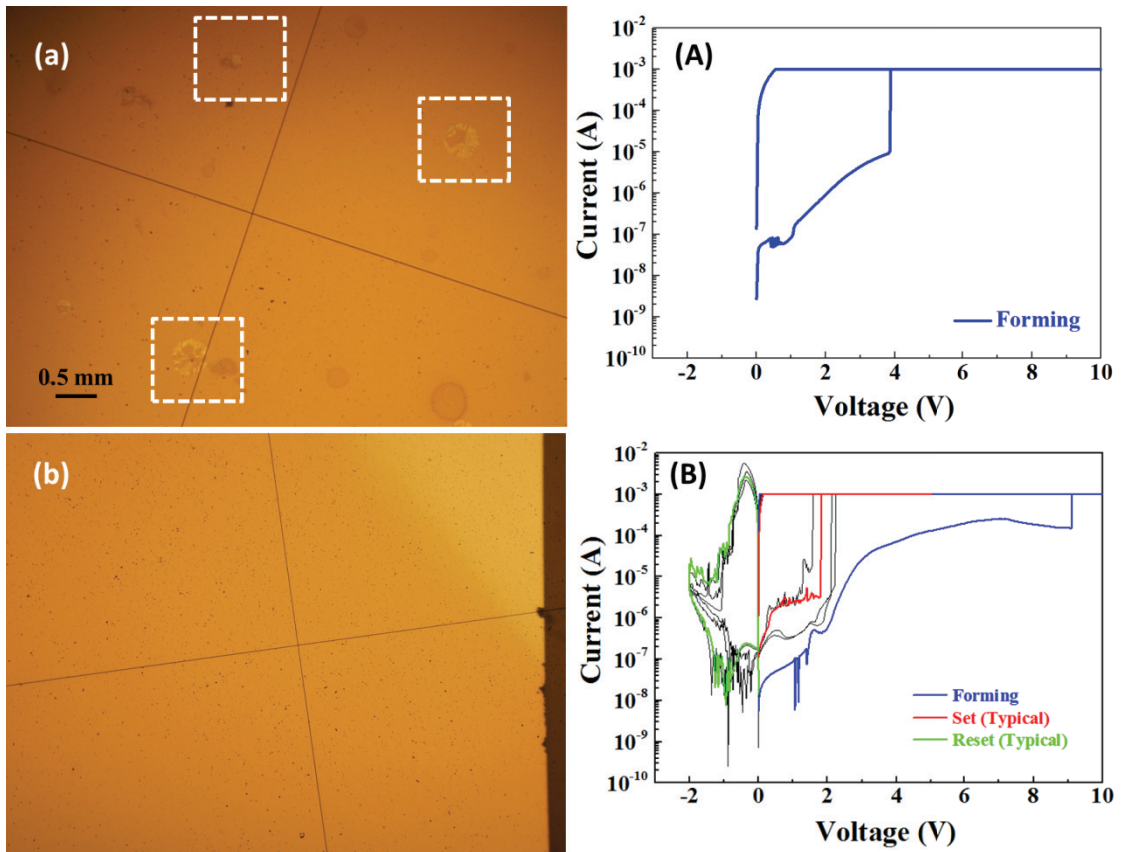**Figure 3-9.** Surface of the HfO$_2$ film after the stress test: Picture (a) shows the results in the presence of water, and picture (b) is the results of IL. Decomposition of the film was visible for (a) at the cubic circles shown by white dotted line, while no decomposed area is observed for (b). *I-V* curve of the stress test is shown at (A) and (B).
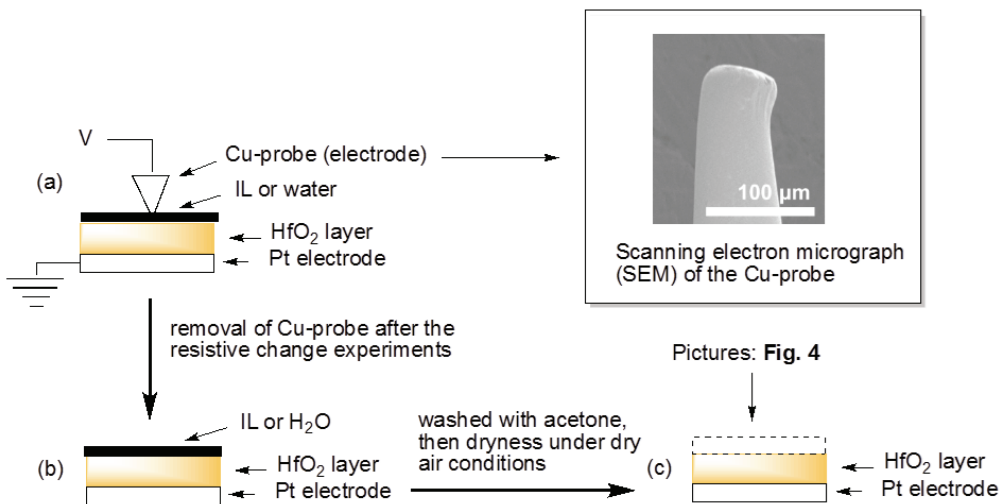
Figure 3-10. Procedure of the stress test.

3-5. Switching behavior

In addition to the reduction of V_{form} and V_{set}, the reduction of a reset current, I_{reset}, which is generally known to supply the relation of $I_{reset} > I_{form}$ and I_{set}, is crucial from a practical point of view. Figure 3-11 shows $1/R_L$ (inverse resistance value at a low resistance state) dependence of I_{reset} for blank, water-, and IL-supplied samples. Not only I_{reset} of blank and water-supplied samples but also I_{reset} of IL-supplied samples satisfies the relation of $I_{reset} \approx 1/R_L$, which is reported as a universal formula for filament type resistive memory devices.[34,35] This result suggests that reset of IL-supplied samples occurs by the same mechanism as other filament type memory devices. Here, it is noted that Ireset of H_2O- and IL-supplied samples are slightly smaller than I_{reset} of blank samples that have the same R_L. Taking into consideration the report by Long et al. that $V_{reset} = I_{reset} \times R_L$ is satisfied for the metallic filament in which the Wiedemann–Franz law holds true,[36] this is consistent with the fact that V_{reset} is reduced by supplying H_2O and IL as shown in Figure 3-1-c.[37] Figure 3-11 indicates that increasing R_L is more effective in reducing I_{reset} than in decreasing V_{set} by supplying solvents. Therefore, making a thin filament with good reproducibility at every set switching is essential for the reduction of I_{reset} and its dispersion. To achieve this, preventing a transient current at the moment of set switching by reducing parasitic capacitance is crucial.[37]
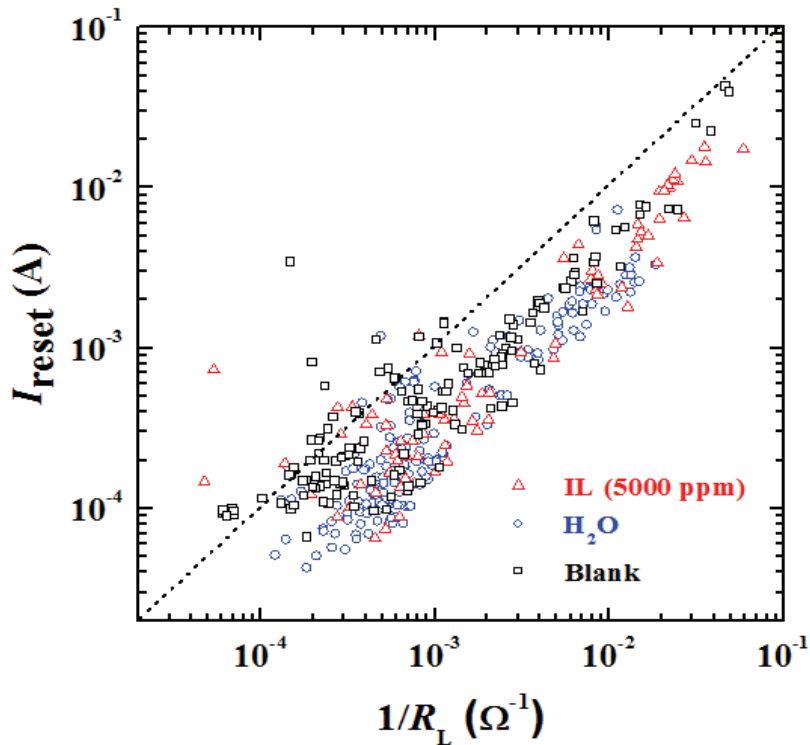
Figure 3-11. $1/R_L$ dependences of Ireset of blank (squares), H_2O- (circles), and IL- (triangles) supplied Cu/HfO$_2$/Pt structures.

3-6. Experimental method

Preparation of Cu/HfO$_2$/Pt cell: Described in Chapter 2.

Current-voltage (I-V) characteristics measurement:

> The *I-V* characteristics were measured using a semiconductor parameter analyzer (Agilent 4155C) in voltage sweep mode at steps of 0.02 V intervals with 640 μs per plot. A current compliance, I_{comp}, was set to 100 μA for all the forming and set processes in this study.

Stress test of the Cu/HfO$_2$/Pt measured in the presence of IL ([bmim][Tf$_2$N]) and water:

> The effect of [bmim][Tf$_2$N] or H$_2$O on forming and set voltage was measured by dropping a small amount of [bmim][Tf$_2$N] (which contains 5,000ppm of ultrapure water) or ultrapure water alone on the HfO$_2$ surface and contacting the HfO$_2$ surface with the Cu-probe in the dropped liquids. [bmim][Tf$_2$N] used in this chapter was purchased from Kanto Chemical Ltd. (Japan) and water content was determined by Karl Fischer method using an 831 KF Coulometer (Metrohm, Ltd.).

3-7. Conclusion of Chapter 3

In summary, we have established that an imidazolium type IL, [bmim][Tf$_2$N] remarkably improved the stability of the electrolyte of a CB-RAM (Cu/HfO$_2$/Pt) and reduced the operating voltage. Voltage operation of the CB-RAM was lower than 10 V has thus been accomplished. At present, the mechanism of how the IL improved stability of electrolyte or water molecules inside the HfO$_2$ pore is still unclear. However, we believe that further investigation of the scope and limitation of this method for improving efficiency of this type of CB-RAM will make it even more valuable.

Chapter 4. Copper Ion Containing Ionic Liquids Provides Improved Endurance and Switching Voltage Distributions of CB-RAM

4-1. The introduction and objective of this study

It was reported that doping of copper metals to the solid electrolyte in the resistive switching memory reduced operation voltages and improved the dispersion of operation voltages and data retention.[38–40] However, the data endurance level worsened with increasing the concentration of the copper doped to the electrolyte due to the formation of filaments which are too thick to be ruptured (to be reset).[40] Inspired by these results, we hypothesized that the addition of an appropriate copper salt solution of IL would improve the switching voltages and data retention as well as the cycling endurance of CB-RAM. This hypothesis based on the expectation that the segregation of copper, which is a main factor causing a reset failure, could be avoided in liquids compared with in solids. We chose [bmim][Tf$_2$N] as a model IL and copper (II) bis(trifluoromethylsulfonyl)amide (Cu(Tf$_2$N)$_2$)[41] as copper salt because this salt has the same anion as that of the IL. In this chapter, we report that addition of a [bmim][Tf$_2$N] solution containing Cu(Tf$_2$N)$_2$ (Cu(Tf$_2$N)$_2$/[bmim][Tf$_2$N]) to the HfO$_2$ layer of a Cu/HfO$_2$/Pt cell effectively improves both the cyclic endurance and operating voltages dispersion of the CB-RAM simultaneously.

4-2. The additive effect of copper containing IL for cyclic endurance

Initially we attempted to optimize the copper salt concentration of Cu(Tf$_2$N)$_2$/[bmim][Tf$_2$N] by evaluating the endurance rate during the switching voltage process: the V_{set} and the V_{reset}. We prepared four kinds of Cu(Tf$_2$N)$_2$/[bmim][Tf$_2$N] samples at Cu ion concentrations of 0, 0.1, 0.2, and 0.4 M, respectively, and investigated the additive effect of the performance of the Cu-probe/HfO$_2$/Pt cell with the DC sweep method (detail explanation was shown in experimental section on this chapter).[27] The copper ion concentrations were determined by chelate titration (the method was explained in section 4-5 of this chapter). We repeated the switching processes (set and reset) up to 100 cycles, and the results of survival rate are shown in Figure 4-1, where one cycle is defined to consist of one reset and one set process. A survival rate suggested that the percentage of cells that can work after each switching cycle and blank indicated the results of the control experiment without any additives. The survival rate of blank samples decreased drastically to 40% after 20 switching cycles, and reached 30% after 100 switching cycles. We found that survival rate after 20 switching cycles was improved to 70% when a 0.1 M Cu(Tf$_2$N)$_2$/[bmim][Tf$_2$N] was added to the cell (triangles in Figure 4-1); however, dropped to 20%, which was rather lower than the survival rate of the blank samples, after 60 switching cycles. On the other hand, the cycling endurance was increased significantly when 0.2 M Cu(Tf$_2$N)$_2$/[bmim][Tf$_2$N] was supplied (diamonds in Figure 4-1): survival rate after 100 switching

cycles reached 70%. It was finally found that the addition of 0.4 M $Cu(Tf_2N)_2$/[bmim][Tf_2N] drastically improved endurance of the cell and the survival rate after repetition of the switching operation of 100 switching cycles (stars in Figure 4-1) reached over 90%. It was reported that the cycling endurance was worsened with increasing the concentration of copper doped to the SiO_2 film of a Cu/SiO_2/Pt structure when copper was singly doped.[40] Therefore our results suggest that supplying copper as a liquid solution is the essence of the enhanced cell endurance. The synergetic effect of copper ion and an IL as solvent has thus been found to increase CB-RAM performance.
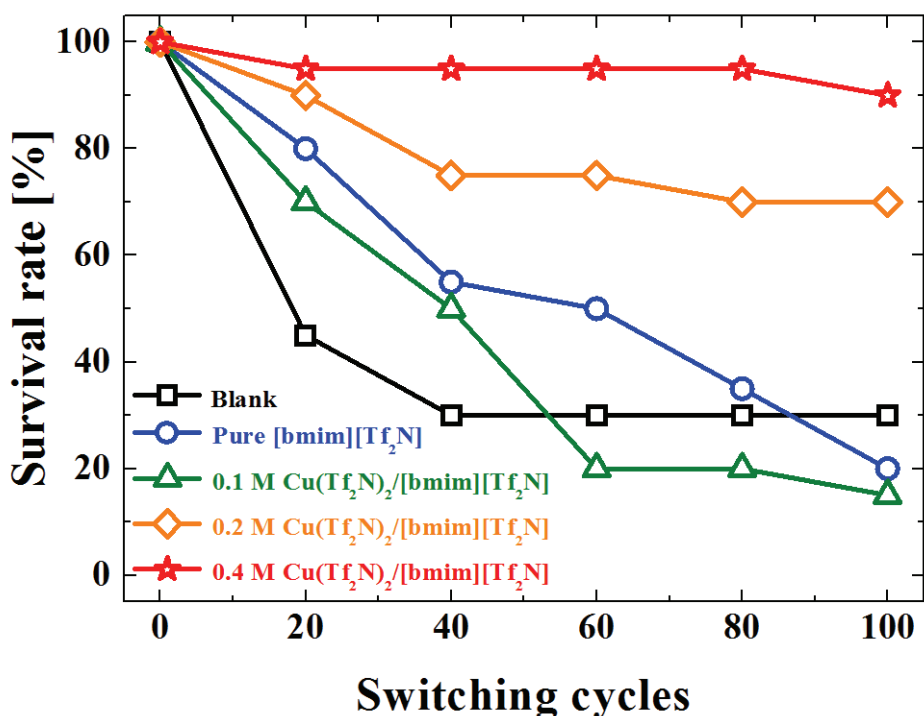

Figure 4-1. Survival rates of Cu/HfO_2/Pt cells measured in the presence of pure [bmim][Tf_2N] and $Cu(Tf_2N)_2$/[bmim][Tf_2N] (Cu 0.1, 0.2 and 0.4 M). "Blank" indicates the results of the control experiment without any additive.

4-3. Switching behavior

We investigated the relationship of the inverse resistance values at a low resistance state ($1/R_L$) versus reset current (I_{reset}). All samples well satisfied the relation of $I_{reset} \approx 1/R_L$, which is reported as a typical formula for filament type resistive memory devices.[34,35] This result indicates that reset of our tested cell occurs with the same mechanism as that of typical filament type memory devices. In particular, a typical error in the cycling endurance of CB-RAM occurs due to reset failure. The main reason of this failure can be attributed to the formation of thick filaments that require large I_{reset}, leading to the destruction of memory cells due to large Joule heat.[40,42] Since the thick filaments might be formed by anomalously large switching voltage that is accidentally caused due to the large V_{set} dispersion of CB-RAM, we next investigated the distributions of V_{set} and V_{reset}.
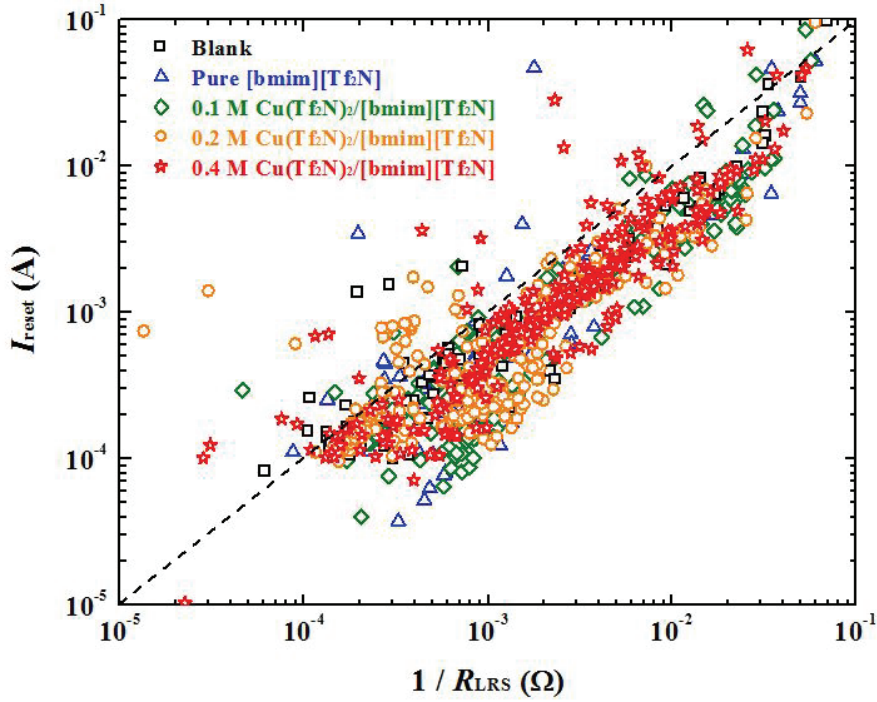
Figure 4-2. $1/R_L$ dependences of I_{reset} of pure [bmim][Tf$_2$N] and Cu(Tf$_2$N)$_2$/[bmim][Tf$_2$N] (Cu: 0.1, 0.2, and 0.4 M).

4-4. The additive effect of copper containing IL for operating voltages value and variances

Figures 4-3 and 4-4 show V_{set} and V_{reset} distributions for various Cu(Tf$_2$N)$_2$ concentrations, respectively. V_{set} widely disperses under the blank condition and under the conditions of adding pure (Cu(Tf$_2$N)$_2$ undoped) [bmim][Tf$_2$N] or 0.1 M Cu(Tf$_2$N)$_2$/[bmim][Tf$_2$N] (Figure 4-3). On the other hand, as anticipated, the dispersions of V_{set} are minimal and are fit well to Gaussian functions (lines

in Figure 4-3) with small standard deviation, when we supplied 0.2 M or 0.4 M Cu(Tf$_2$N)$_2$/[bmim][Tf$_2$N] (Figure 4-5). This means that accidental generation of anomalously large V_{set} is suppressed under the conditions of adding 0.2 M or 0.4 M Cu(Tf$_2$N)$_2$ /[bmim][Tf$_2$N]. Therefore, supplying the Cu containing IL is suggested to reduce the dispersion of V_{set} by enhancing the filament growth while avoiding the segregation of copper. The same trend as observed in the V_{set} distribution is confirmed in the V_{reset} distribution (Figure 4-4). In particular, σ for the V_{reset} distribution under the condition of adding 0.4 M Cu(Tf$_2$N)$_2$/[bmim][Tf$_2$N] is very small (Figure 4-5), suggesting that the dispersion of the filament thickness is reduced as a result of the small V_{set} dispersion. However, it is noticed that the average value of V_{set} increases with increasing copper concentration. In particular, the average V_{set} for 0.4 M Cu(Tf$_2$N)$_2$/[bmim][Tf$_2$N] was 0.1 V larger than that of pure IL condition (Figure 4-6). We assume that this can be attributed to the increase in viscosity of the IL solution including the copper salt. In fact, the viscosity of ILs was increased with increasing the concentration of solutes (Figure 4-7 and Table 4-2). Therefore, reducing the dispersion of V_{set} and suppressing the generation of anomalously large V_{set} is crucial in the improvement of the cycling endurance.
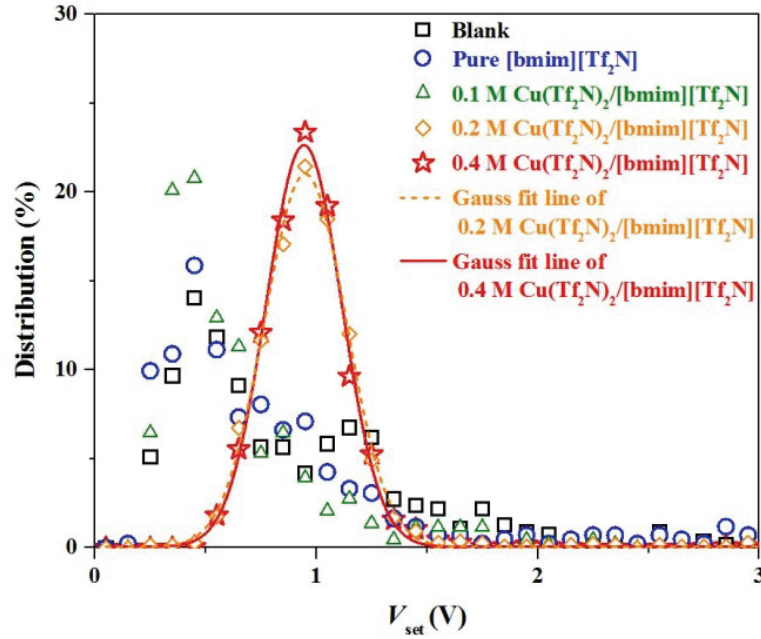
Figure 4-3. V_{set} distributions of Cu/HfO$_2$/Pt cells measured in the presence of pure [bmim][Tf$_2$N] and Cu(Tf$_2$N)$_2$/[bmim][Tf$_2$N] (Cu 0.1, 0.2 and 0.4 M). "Blank" indicates the results of the control experiment without any additive.
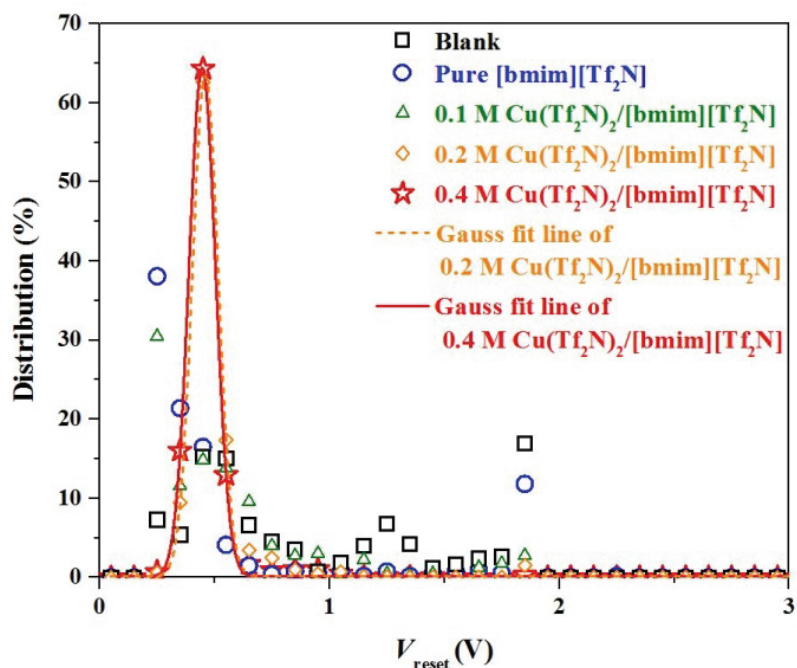
Figure 4-4. V_{reset} distributions of Cu/HfO$_2$/Pt cells measured in the presence of pure [bmim][Tf$_2$N] and Cu(Tf$_2$N)$_2$/[bmim][Tf$_2$N] (Cu 0.1, 0.2 and 0.4 M). "Blank" indicates the results of the control experiment without any additive.
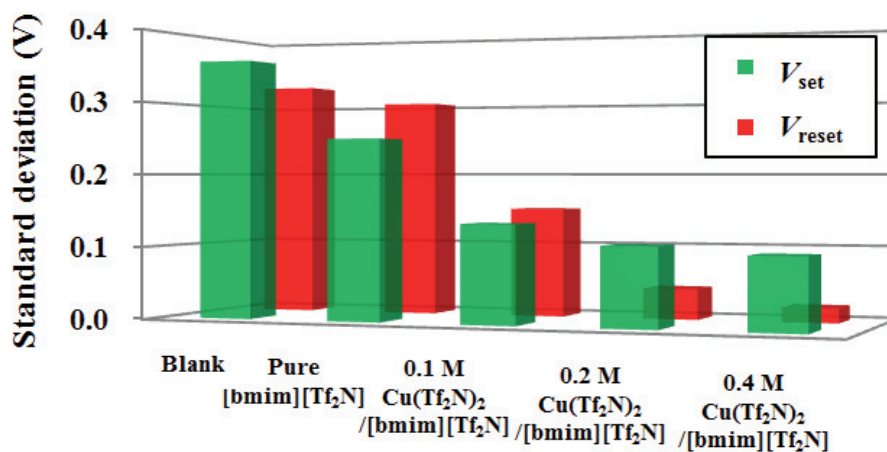
Figure 4-5. V_{set} and V_{reset} variances of Cu/HfO2/Pt cells measured in the presence of pure [bmim][Tf$_2$N] and Cu(Tf$_2$N)$_2$/[bmim][Tf$_2$N] (Cu 0.1, 0.2 and 0.4 M). "Blank" indicates the results of the control experiment without any additive.
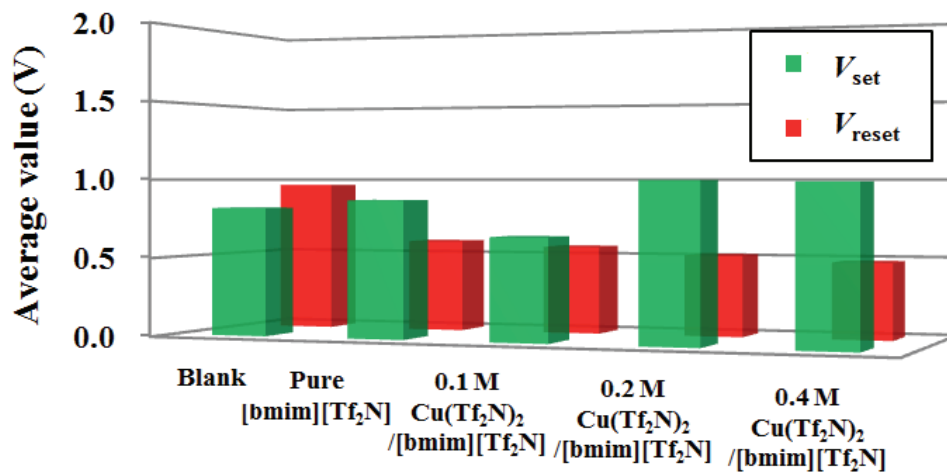
Figure 4-6. V_{set} and V_{reset} average values of Cu/HfO$_2$/Pt cells measured in the presence of pure [bmim][Tf$_2$N] and Cu(Tf$_2$N)$_2$/[bmim][Tf$_2$N] (Cu 0.1, 0.2 and 0.4 M). "Blank" indicates the results of the control experiment without any additive.

Table 4-1. Values used in Figures 4-5 and 4-6.

Additive	V_{set} [V]		V_{reset} [V]	
	average value	standard deviation	average value	standard deviation
Blank	0.82	0.36	0.96	0.33
Pure [bmim][Tf$_2$N]	0.87	0.25	0.59	0.30
0.1 M Cu(Tf$_2$N)$_2$/[bmim][Tf$_2$N]	0.65	0.13	0.56	0.15
0.2 M Cu(Tf$_2$N)$_2$/[bmim][Tf$_2$N]	1.00	0.11	0.51	0.04
0.4 M Cu(Tf$_2$N)$_2$/[bmim][Tf$_2$N]	0.99	0.10	0.48	0.02
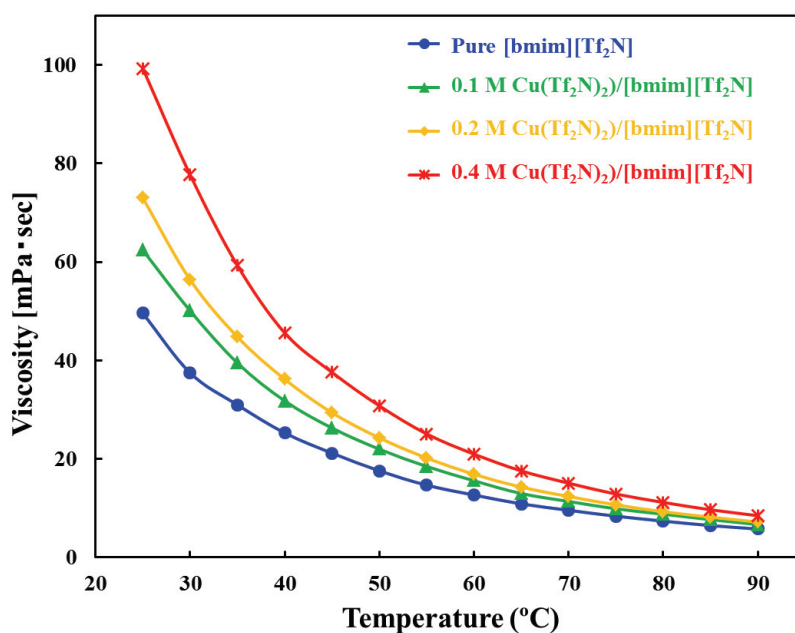
Figure 4-7. Viscosities of pure [bmim][Tf$_2$N] and Cu(Tf$_2$N)$_2$/[bmim][Tf$_2$N] (Cu 0.1, 0.2 and 0.4 M).

Table 4-2. Viscosities of pure [bmim][Tf$_2$N] and Cu(Tf$_2$N)$_2$/[bmim][Tf$_2$N] (Cu 0.1, 0.2 and 0.4 M).

Temperature (°C)	Viscosity (mPa·sec)			
	Pure [bmim][Tf$_2$N]	Cu(Tf$_2$N)$_2$/[bmim][Tf$_2$N]		
		0.1 M	0.2 M	0.4 M
25	49.6	62.4	73.0	99.3
30	37.5	50.1	56.4	77.7
35	31	39.5	44.8	59.3
40	25.3	31.8	36.2	45.6
45	21.2	26.3	29.4	37.6
50	17.6	22.0	24.3	30.8
55	14.7	18.5	20.2	25.1
60	12.7	15.6	16.9	21.0
65	10.9	13.0	14.3	17.6
70	9.6	11.4	12.4	15.1
75	8.4	9.9	10.7	12.9
80	7.4	8.8	9.3	11.2
85	6.5	7.7	8.2	9.7
90	5.8	6.7	7.2	8.5

Table 4-3. Physicochemical properties of copper ion containing ILs

Copper ion containing IL	Ionic conductivity σ_i /30 °C [mS/cm]	Viscosity η /25 °C [mPa·sec]
[bmim][Tf$_2$N]	4.71	49.6
0.1 M Cu(Tf$_2$N)$_2$/[bmim][Tf$_2$N]	4.46	62.4
0.2 M Cu(Tf$_2$N)$_2$/[bmim][Tf$_2$N]	3.38	73.0
0.4 M Cu(Tf$_2$N)$_2$/[bmim][Tf$_2$N]	2.83	99.3

4-5. Experimental method

Preparation of Cu/HfO$_2$/Pt cell: Described in Chapter 2.

Current-voltage (I-V) characteristics measurement:

The *I-V* characteristics were measured using a semiconductor parameter analyzer (Agilent 4155C) in voltage sweep mode at steps of 0.02 V intervals with 640 µs per plot. A current compliance, I_{comp}, was set to 100 µA for all the forming and set processes in this study.

Preparation of Cu(Tf$_2$N)$_2$/[bmim][Tf$_2$N]:

The Cu(Tf$_2$N)$_2$ and [bmim][Tf$_2$N] were mixed with measuring flask, and shaken several minutes until completely dissolved. These operations were performed in a nitrogen-filled glove box.

Concentration determination method of Cu(Tf$_2$N)$_2$/[bmim][Tf$_2$N]:

The concentration of Cu(Tf$_2$N)$_2$/[bmim][Tf$_2$N] solutions were determined following chelate titration method. Each Cu(Tf$_2$N)$_2$/[bmim][Tf$_2$N] solutions were diluted with mixed solution of Methanol/H$_2$O (3/7 v/v) to be 0.01 M concentration, and 1-(2-pyridylazo)-2-naphthol (PAN) was dissolved to each solution as the indicator. The copper concentrations in the solution were determined by titration with 0.01 M aqueous solution of ethylenediaminetetraacetic acid disodium salt (EDTA). The EDTA reagent was dried in vacuo prior to use. The structures of reagents for chelate titration were described in Scheme 4-1.

Scheme 4-1. The reagents for chelate titration

EDTA   PAN

31
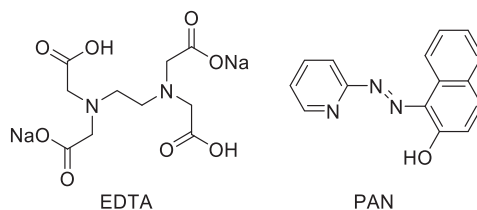
4-6. Conclusion of Chapter 4

In summary, the improvement of cycling endurance and operating voltages dispersion was accomplished by addition of a $Cu(Tf_2N)_2$/[bmim][Tf_2N] to the HfO_2 film of Cu/HfO_2/Pt cell. First, by doping copper as a liquid solution, the reduction in the V_{set} dispersion is considered to be achieved by enhancing the filament growth while avoiding the segregation of copper. Then, the improvement of the cycling endurance was suggested to be brought about by the suppression of the generation of anomalously large V_{set}. Although a slight increase of V_{set} was caused when $Cu(Tf_2N)_2$/[bmim][Tf_2N] was supplied to the HfO_2 film, we believe that high degree of freedom in design of IL enables solving this problem.

Chapter 5. Influence of Ionic liquids physicochemical properties for the Performance Improvements of CB-RAM.

5-1. *The introduction and objective of this study*

We investigated effects of 18 types ILs on the CB-RAM (Cu/HfO$_2$/Pt) cell to reveal relationship between physicochemical properties of the ILs and switching characteristics of the CB-RAM.

5-2. *ILs for this study*

The tested 18 types of ILs are as follows; [emim][Tf$_2$N], emim][Tf$_2$N], [bmim][Tf$_2$N], [hmim][Tf$_2$N], [omim][Tf$_2$N], [bdmim][Tf$_2$N], [MEmim][Tf$_2$N], [bmtr][Tf$_2$N], [N$_{1224}$][Tf$_2$N], [PP$_{14}$][Tf$_2$N], [Py$_4$][Tf$_2$N], [bmim][FSA], [bmim][BF$_4$], [bmim][PF$_6$], [bmim][DCA], [bmim][TfO], [bmim][MeSO$_4$], [bmim][Me$_2$PO$_4$] and [emim][(HF)$_{2.3}$F]. Their structures are shown in Scheme 5-1, and synthetic methods are described in Chapter 7.

Scheme 5-1. List of ILs used in this study.

33
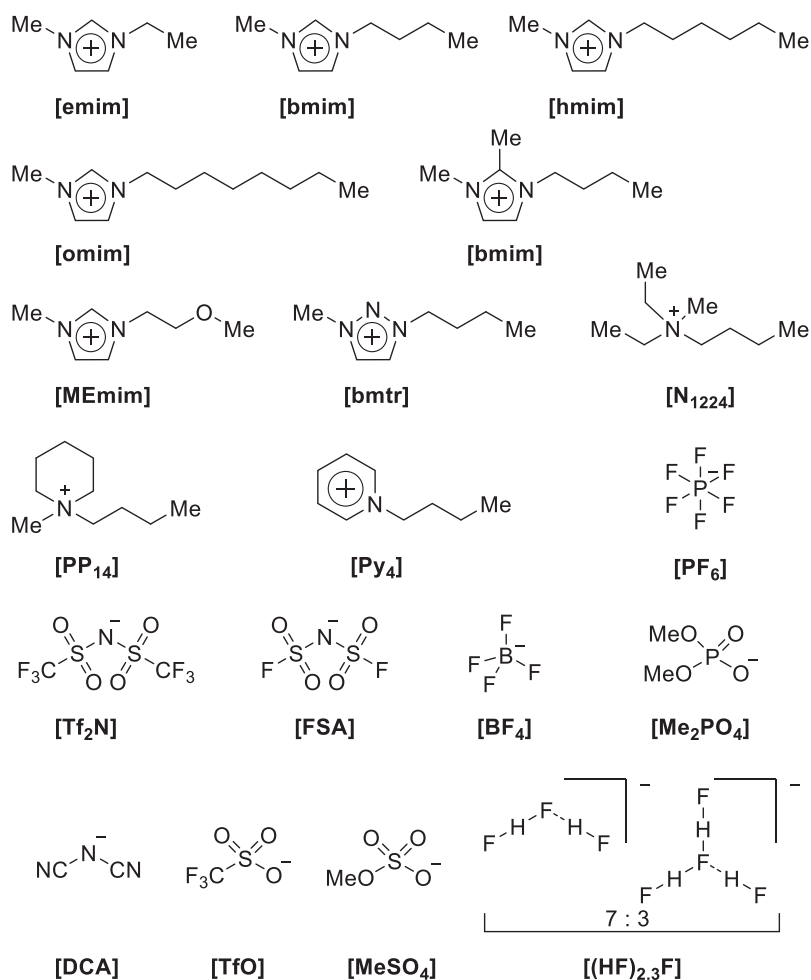
5-3. Switching behavior

We have investigated at the switching characteristics of the Cu/HfO$_2$/Pt cell using various types of ILs as additives. Since the influence of the IL-addition to the metal oxide layer of the CB-RAM on the reset process is unclear, we investigated the $1/R_L$ dependence of I_{reset} (I_{reset}-$1/R_L$), where R_L and I_{reset} are the low resistance state and the reset current, respectively. Figure 5-1a shows the dependence of I_{reset}-$1/R_L$ on the anionic species of the IL which is restricted to [Tf$_2$N]. On the other hand, Figure 5-1b shows the dependence of I_{reset}-$1/R_L$ on the anionic species of the IL which cationic species of the IL is restricted to [bmim]. Figures 5-1a and 1b show that the relationship of $I_{reset} \approx 1/R_L$, which is reported as a universal formula for filament type resistive memory devices[34,35] holds true for the IL-added CB-RAM. Figures 5-1a and 1b also indicate that the increase in R_L causes the reduction of I_{reset} independent of the types of ILs.

Next, we investigated the V_{set} dependence of R_L (R_L-V_{set}). Figure 5-2a shows the dependence of R_L-V_{set} on the cationic species of IL which is restricted to [Tf$_2$N]. On the other hand, Figure 5-2b shows the dependence of R_L-V_{set} on the anionic species of the IL which is restricted to [bmim]. Figures 5-2a and 2b show that R_L increases with the decreasing V_{set} independent of the types of ILs. These results suggest that the R_L values can be increased by decreasing V_{set}, resulting in a decrease of Ireset following the relationship of I_{reset}-$1/R_L$ shown in Figure 5-1. Since I_{reset} is the maximum current that is necessary to induce resistive switching, reducing V_{set} to reduce I_{reset} is crucial in lowering the power consumption. In ReRAM devices, it is reported that a high V_{set} causes a high transient current and makes a thick filament, which requires a high current to become the reset state.[43] Our results suggest that the same mechanism relating Ireset with Vset is applicable to the IL-added CB-RAM. Therefore, it is also expected that retaining V_{set} at a low value is crucial to ensure reproducible resistive switching.[37]
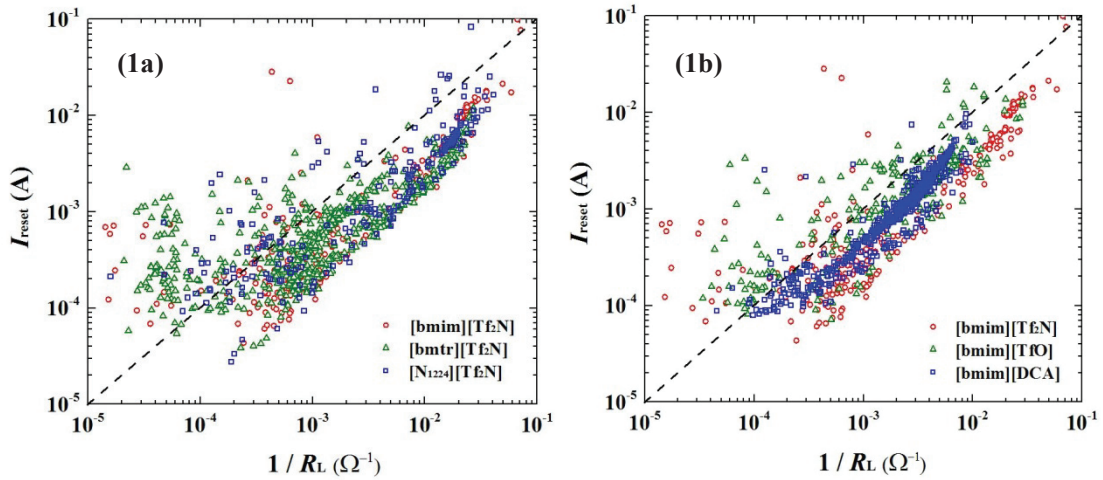

Figure 5-1. $1/R_L$ dependences of Ireset for IL supplied the Cu/HfO$_2$/Pt cell.
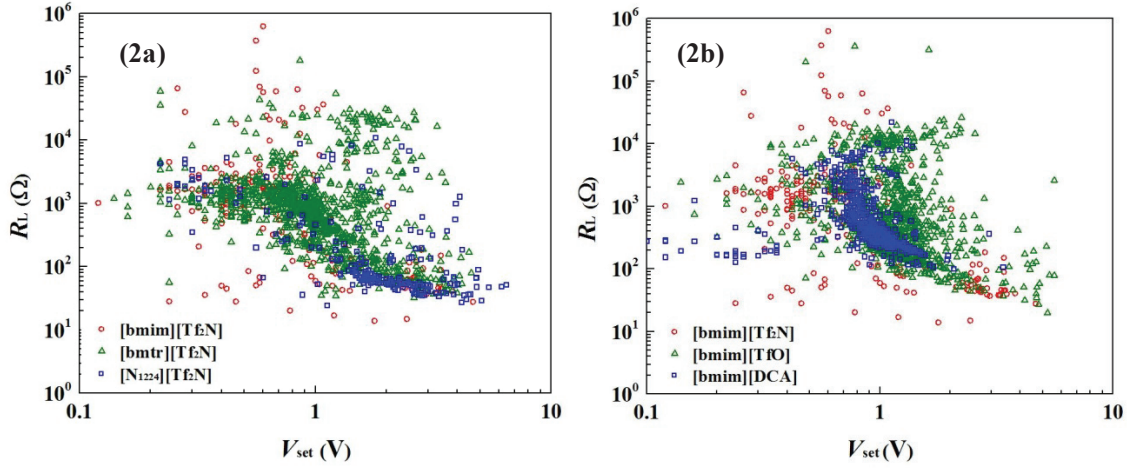
Figure 5-2. V_{set} dependences of R_L for IL supplied the Cu/HfO$_2$/Pt cell.

5-4. Addition effect of pure ILs on the switching voltages of the Cu/HfO$_2$/Pt cell

We next investigated the relationship between the physicochemical properties of the ILs and the V_{set} values. First, we focused on the ionic conductivity of the ILs, because metal filaments might be easily produced in the ILs that have high ionic conductivities. Figure 5-3 shows the dependence of V_{set} on the ionic conductivity of the IL (σ_i) Here, σ_i was measured by the complex-impedance method using the following equation: $\sigma_i = J / R_{sol}$ [mS/cm], where J is the cell constant (cm^{-1}) and R_{sol} is the resistance of the bulk IL at a high frequency limit. A low R_{sol} (high σ_i) suggests that Cu ions in the IL can rapidly diffuse.[1]

Since V_{set} can vary between different wafers even if prepared under the same conditions, in this study, we used the ΔV_{set} values calculated by the following equation using the wafer to which [bmim][Tf$_2$N] was added as a standard sample: $\Delta V_{set} = (V_{set}) - $ (average V_{set} of [bmim][Tf$_2$N]-added sample), where V_{set} was measured for samples on the same wafer. The error bars in Figure 5 show 75 to 25% of all the ΔV_{set} values from the minimum ΔV_{set} value, for each IL to avoid using illegular results for evaluation.

The ΔV_{set} values decreased with the increasing σ_i except for [bmim][DCA] as shown in Figure 5-3. It is reported that [emim][(HF)$_{2.3}$F] possesses the extremely high σ_i of 100 mS/cm. As expected, the lowest ΔV_{set} value was recorded for this IL (Figure 5-3, #18), although the [emim][(HF)$_{2.3}$F] frequently caused switching errors. We already mentioned that the HfO$_2$ layer decomposed due to the electrochemical decomposition of water based on its low electrochemical stability.[44] The frequent switching error may be attributed to the lower electrochemical stability of [emim][(HF)$_{2.3}$F] than that of [bmim][Tf$_2$N].[15] In fact, we observed the generation of gas from [emim][(HF)$_{2.3}$F] by applying a voltage within ±2 V. ILs

that possess a high σ_i roughly have low ΔV_{set} values and the combination of an imidazolium family cation with the [Tf$_2$N] or [FSA] anion has been found to be a good additive to the Cu/HfO$_2$/Pt cell; [emim][Tf$_2$N], [bmim][Tf$_2$N] and [bmim][FSA] were the best ILs to reduce the V_{set} values. As can be seen in Figure 5-3, deviations in the ΔV_{set} values of suitable ILs, [bmim][Tf$_2$N], [emim][Tf$_2$N], and [bmim][FSA] are less than 0.5 V. Although [bmim][DCA](#12) was also expected to show a low V_{set} because of its high σ_i, the obtained ΔV_{set} value was not sufficiently low, contrary to expectation. This suggests that ΔV_{set} is not determined only by the ionic conductivity.
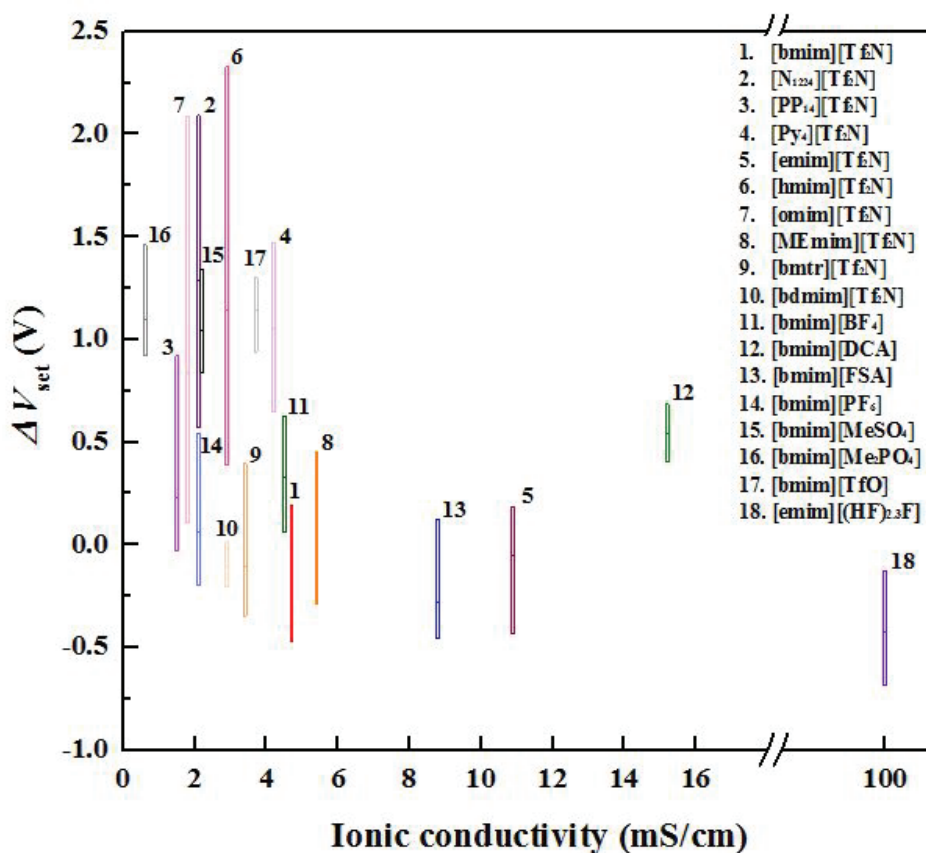
Figure 5-3. ΔV_{set} dependence between ionic conductivities of 18 types of ILs for the Cu/HfO$_2$/Pt cell during the switching process.

Katayama and co-workers reported that an over potential was observed for the electrodeposition of Co species with an amide-type IL and this was attributed to the coordination of the anion derived from the IL.[45] Hence, we assumed that a high ΔV_{set} might be caused by the strong coordinating ability of the [DCA] anion towards the Cu ion. To confirm this hypothesis, we looked at the relationship between the basicity (β value) of the ILs and ΔV_{set} values

(Figure 5-4). The β value is a solvatochromic parameter and indicates the proton accepting ability of the ILs, and it also corresponds to the coordinating ability of the anion moiety to a metal cation.[46] In fact, ΔV_{set} increased with the increase in the β value and the highest ΔV_{set} was observed for [bmim][Me$_2$PO$_4$], which has the highest β value, as shown in Figure 5-4. From the results shown in Figures 5-3 and 5-4, it was thus concluded that increasing σ_i and decreasing β of the IL might be important in order to reduce the V_{set} values.
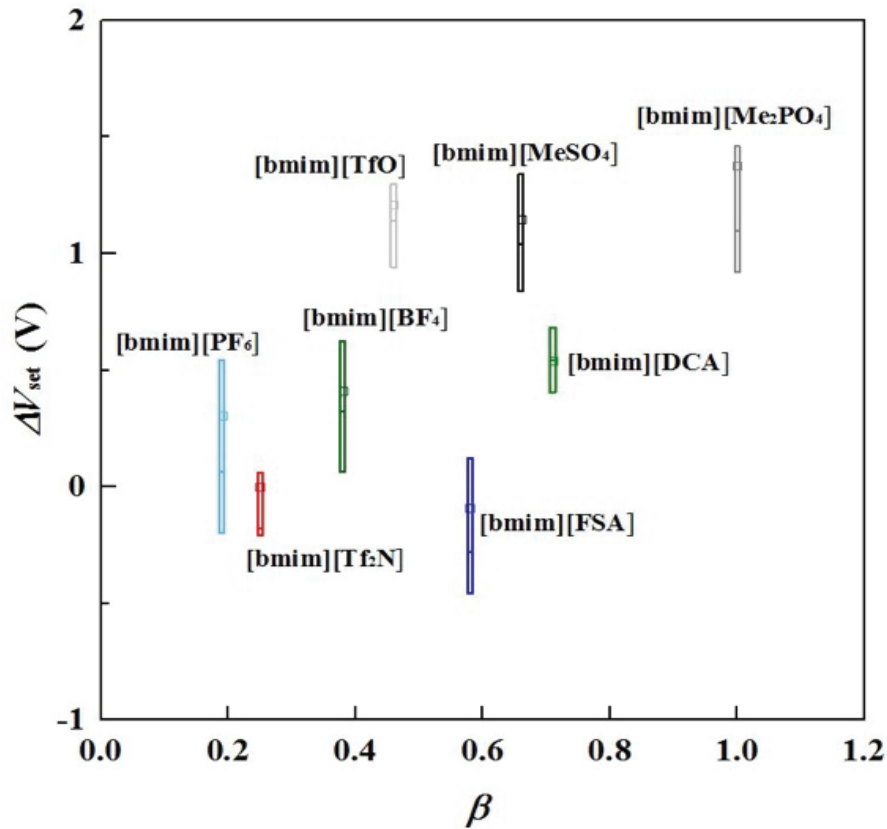
Figure 5-4. The relationship of ΔV_{set} to the β values of ILs.

5-5. Addition effect of Cu ion-containing ILs on the switching voltage values and endurance of Cu/HfO₂/Pt cell

It was reported that the doping of Cu ions in a solid electrolyte in a resistive switching memory reduced the operating voltages and improved the variability of these voltages and data retention.[40] However, the data endurance became worse with the increasing concentration of Cu doped in the electrolyte.[40] We investigated the addition effect of a Cu salt solution of the IL on the operating voltages and data retention as well as the cycling endurance of the CB-RAM. As expected, the im-

provement of the cycling endurance and the variability of the operating voltages was accomplished by the addition of $Cu(Tf_2N)_2$/[bmim][Tf_2N] to the HfO_2 film of the Cu/HfO_2/Pt cell (see chapter 4).[47] However, it was found that the average value of V_{set} slightly increased with the increasing Cu ion concentration; the average V_{set} for 0.4 M $Cu(Tf_2N)_2$/[bmim][Tf_2N] was 0.1 V higher than that of the pure IL-added samples as shown in Figure 4-6.[47] We also measured σ_i of the $Cu(Tf_2N)_2$/[bmim][Tf_2N] for each Cu concentration. The conductivities were determined to be 4.7, 4.5, 3.4, and 2.8 mS/cm for the pure [bmim][Tf_2N], 0.1 M, 0.2 M and 0.4 M $Cu(Tf_2N)_2$/[bmim][Tf_2N], respectively. It was assumed that this reduction of σ_i might be caused by the increased viscosities following the Walden's law[14] (Figure 4-7). Thus, the tendency that an average V_{set} slightly increases with the increase in the Cu ion concentration is consistent with the tendency of the experimental results shown in Figure 5-3. In order to investigate in more detail, we measured Z of the $Cu(Tf_2N)_2$/[bmim][Tf_2N] for each Cu ion concentration. The Nyquist plots of Z are shown in Figure 5-5. The results show that R_{sol} (inset of Figure 5-5) increases and a charge transfer resistance (R_{ct}) (Figure 5-5) decreases with the increasing Cu ion concentration. Since the ΔV_{set} increases with the increase in the Cu ion concentration, it is suggested that R_{sol} and R_{ct} are competing with each other with respect to increasing V_{set} by the Cu ion doping; the decline in the Cu ion diffusion was more dominant than the enhancement of the Cu ionization. It has been reported that σ_i ($\propto R_{sol}$) is proportional to the ion concentration and the inverse of the viscosity.[1] Hence, we investigated the relationship of the molar concentrations or the viscosities of the ILs to the ΔV_{set} values; however, we found no relationship between them (Figures 5-6 and 5-7). On the other hand, the dependence of V_{reset} on the Cu ion concentration is weak as shown in Figure 4-6. V_{reset} slightly decreases with the Cu ion concentration. This result suggests that the electrochemical reaction does not play an important role in the reset process as was the case in the pure IL-added samples. It is reported that the rupture of the filament at the reset process occurred by Fick diffusion, which is a physical phenomenon and is enhanced by Joule heating.[23,25,40,42] Thus, both the kind of ILs and the Cu ion concentration contained in the ILs slightly influence V_{reset}.

Next, we also investigated the correlation between the variability of the operating voltages and the physicochemical properties of the ILs such as σ_i, viscosity, and polarity. As mentioned, we recently reported that improvement of the cycling endurance and variability of the operating voltages has been achieved by the addition of $Cu(Tf_2N)_2$/[bmim][Tf_2N] to the HfO_2 film layer of a Cu/HfO_2/Pt cell.[47] The endurance was remarkably increased with the increasing Cu ion concentration. To elucidate the endurance improvement, we investigated the relationship between I_{reset} and $1/R_L$ (Figure 4-2), and we obtained the same tendency as the pure ILs (Figures 3-1, 5-1 and 5-2). It has thus been established that the optimized IL system, [bmim][Tf_2N] including $Cu(Tf_2N)_2$, showed very narrow deviation for the relationship of I_{reset} and $1/R_L$ as shown in Figure 4-2.

It is known that Cu^+ is more stable than Cu^{2+} in an IL solution, while no such reaction occurs in an aqueous solution,[41,48] thus the comproportionation reaction could occur as follows: $Cu^{2+} + Cu^0 \rightarrow$ $2Cu^+$. This reaction could induce the rupture of the Cu filament during the reset process, but Figure 4-2 showed the same tendency for the pure IL ones (Figures 3-1, 5-1 and 5-2). This result suggests that the comproportionation reaction did not affect the reset process. Additionally, as mentioned above, the V_{reset} values were not strongly affected by the electrochemical property of the ILs. Thus, enhancement of the endurance improvement should be caused by another factor. Next, we looked at the variability of the results. The V_{set} widely varies under no additive conditions, and the conditions of adding pure [bmim][Tf$_2$N], and 0.1 M Cu(Tf$_2$N)$_2$/[bmim][Tf$_2$N] (Figure 4-5).[47] On the other hand, the variability of V_{set} was minimal when 0.2 M and 0.4 M Cu(Tf$_2$N)$_2$/[bmim][Tf$_2$N] were added as shown in Figure 4-5. This means that the generation probability of the Cu filaments that provides anomalously high V_{set} values is suppressed by adding 0.2 M or 0.4 M Cu(Tf$_2$N)$_2$/[bmim][Tf$_2$N]. Therefore, the Cu-containing IL is suggested to reduce the dispersion of V_{set} by enhancing the filament growth while avoiding the segregation. A similar trend of the V_{set} distribution was also found in the V_{reset} distribution (Figure 4-5).[47] Chin and co-workers reported that whereas the switching voltages were reduced, the cycling endurance was reduced by increasing the amount of Cu which was doped in the SiO$_2$ film in a Cu/SiO$_2$/Pt cell. The authors described that the condensation of Cu ion and the formation of a thick filament might be a reason for the poor endurance.[40] This is in contrast to the result of the present study, in which the cycling endurance was remarkably improved in exchange for the small increase in V_{set} by supplying Cu(Tf$_2$N)$_2$/[bmim][Tf$_2$N] to the HfO$_2$ layer of a Cu/HfO$_2$/Pt cell.[47]
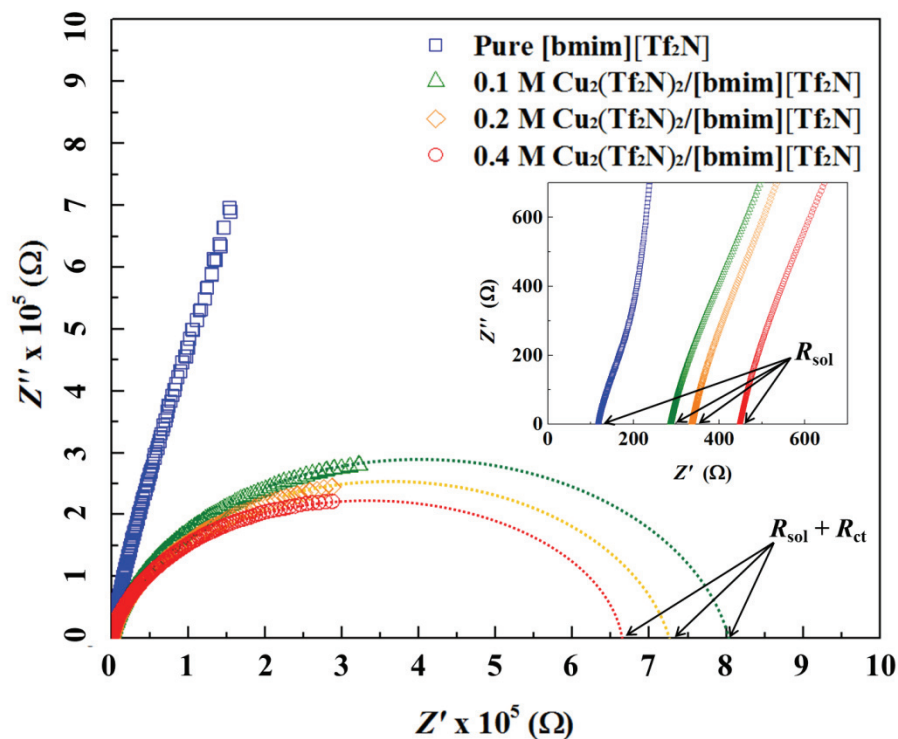
Figure 5-5. Nyquist plots measured by impedance analysis of pure [bmim][Tf$_2$N] and Cu(Tf$_2$N)$_2$/[bmim][Tf$_2$N] (Cu: 0.1, 0.2, and 0.4 M).
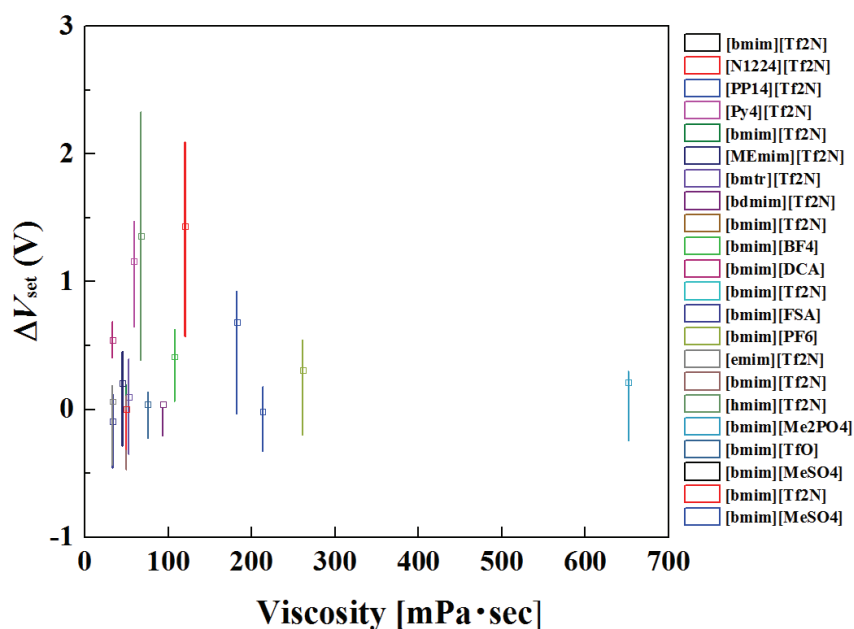

Figure 5-6. Relationship between ΔV_{set} and viscosities of ILs
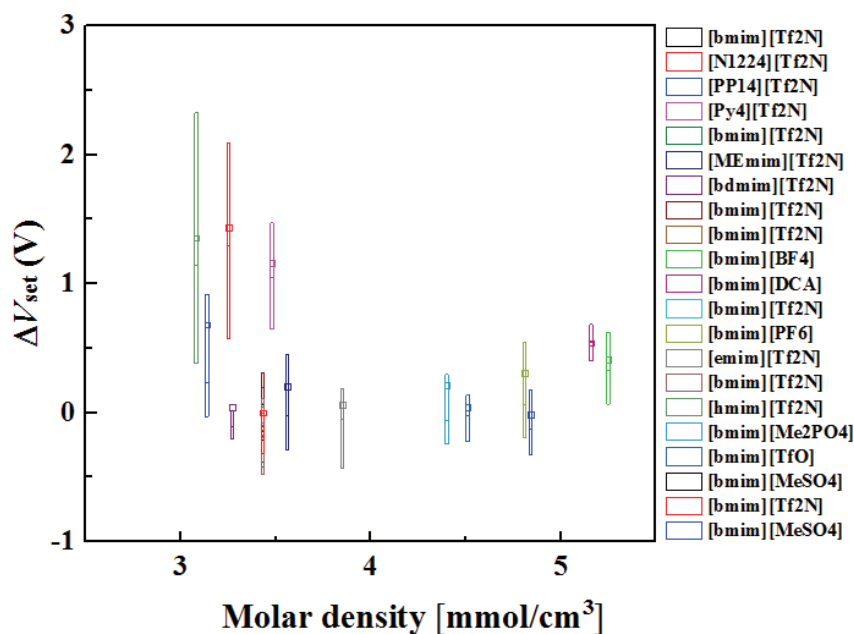
Figure 5-7. Relationship between ΔV_{set} and molar density of ILs

5-6. The role of HfO₂

In order to investigate the role of HfO_2, we conducted control experiments without the HfO_2 layer and obtained unanticipated results: a hysteresis property was observed as shown in Figure 5-8 when a Cu probe came into contact with an IL that was dropped on a Pt electrode at a distance of 125 μm from the electrode to form a Cu/IL (125 μm)/Pt cell. To elucidate the origin of the hysteresis, we measured *I-V* characteristics in two different voltage sequences, that is, sequence 1 (0 V→ +15 V→ 0 V → -2 V → 0 V) and sequence 2 (0 V→ -15 V→ 0 V → +2 V → 0 V). The results obtained by both sequences were superimposed on the same graph in Figure 5-9, where a positive/negative of the *I-V* characteristics obtained by the sequence 2 was inverted. As can be seen in Figure 5-9, a similar hysteresis property as observed with sequence 1 was obtained with sequence 2. If the origin of the hysteresis had been provided by the generation and rupture of Cu filaments, *I-V* characteristics by sequence 2 should not give the hysteresis curve because the ionization of Cu proceeds only when a positive bias is applied to the Cu probe. In addition, it should be noticed that the peaks indicated by the red arrows in Figure 5-8 appear only in *I-V* characteristics obtained with sequence 1, suggesting that the Cu probe was indeed dissolved in the IL due to generation of Cu^{n+} ions when the positive bias was applied to the Cu probe. Therefore, it is suggested that the charge and discharge of the electric double layer is slow owing to the viscous nature of the IL, giving the hysteresis in the *I-V* characteristics. These results indicate that the main

role of HfO_2 might be as both the cage and scaffold of the Cu filament: since sufficient concentration of Cu^{n+} ions is maintained in the cage and effectively guided along the pores of the HfO_2, smooth generation and rupture of the Cu filaments might take place on the wall inside the pores which is filled with the IL. At present, however, no further role of the HfO_2 has been identified.
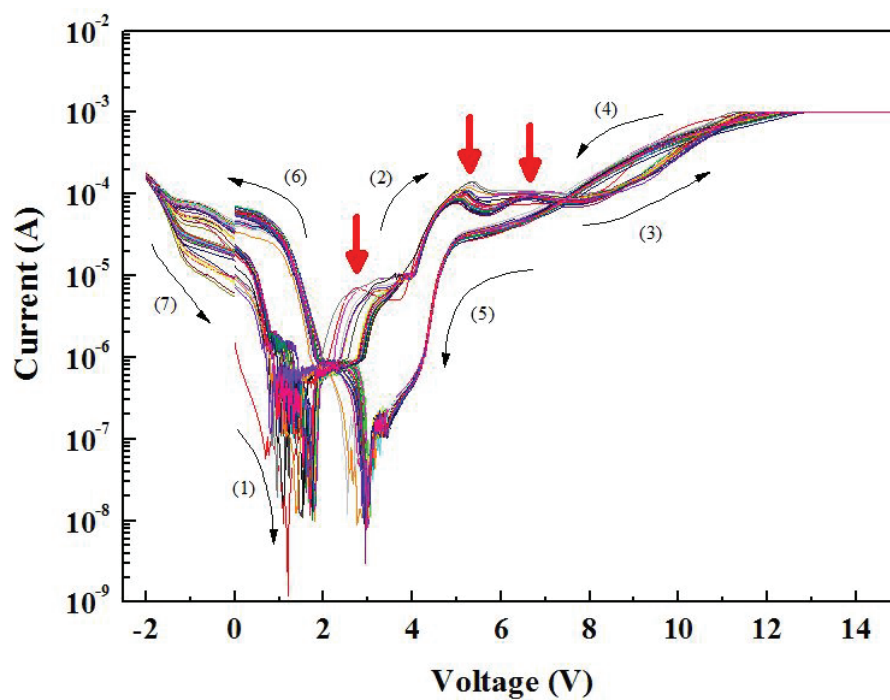

Figure 5-8. *I-V* curve of the Cu/ IL ([bmim][Tf_2N])/ Pt cell in which the IL had been placed on the surface of the Pt electrode. The results were obtained by sequence 1.
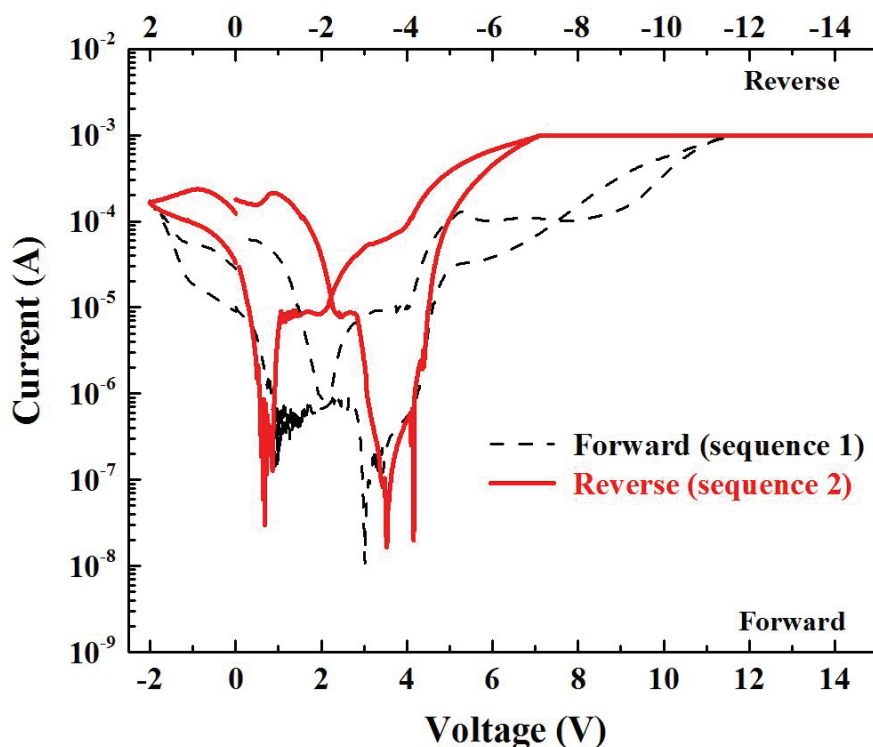
Figure 5-9. *I-V* curve of the Cu/ IL ([bmim][Tf$_2$N])/ Pt cell under the two conditions of sequences 1 and 2.

5-7. Experimental method

Preparation of Cu/HfO$_2$/Pt cell: Described in Chapter 2.

Current-voltage (I-V) characteristics measurement:

A drop of IL (ca. 0.1 μL) was added to the surface of the HfO$_2$ film and then the Cu-probe was brought into contact with the surface through the IL droplet. All the measurements were performed under flowing nitrogen to avoid water absorption into the ILs. The current-voltage (*I-V*) characteristics were measured using a semiconductor parameter analyzer (Agilent 4155C) in the DC sweep mode at 0.02 V intervals with 640 μs per plot. A current compliance value, I_{comp}, at which a current flowing through CB-RAM cell is limited, was fixed at 100 μA for all the forming and set processes in this study. Because of the ease of experiments, we put a drop of the IL on the surface of HfO$_2$. Since the size of each HfO$_2$ pore was reported to be ca. 2~5 nm and the wall width between pores was around 10 nm[28] (Figure 2-9.). Therefore, the necessary volume of the IL which could completely fill up the inside of the HfO$_2$ film is estimated to be less than 9.2 x 10^{-5} μL when we use a film which is 1.0 square centimeter and 12 nm thick.

Preparation of ILs: Described in Chapter 7.

Physicochemical property measurement of IL: Described in Chapter 8.

5-8. Conclusion of Chapter 5

We investigated the addition effect on the performance of the Cu/HfO$_2$/Pt cell as CB-RAM using 18 types of ILs, and found that the operating voltage was significantly reduced by supplying a trace amount of the ILs to the HfO$_2$ layer of the Cu/HfO$_2$/Pt cell. It was revealed that the switching mechanism of the present IL-added CB-RAM is explained by a filament mechanism which holds true for the CB-RAM without IL-addition independent of the type of IL. Both increasing σ_i and decreasing the β value of the additive IL are important in reducing V_{set}, whereas forming a thin filament is important in reducing V_{reset} (Figure 5-10). Among the tested ILs, [bmim][Tf$_2$N], [emim][Tf$_2$N] and [bmim][FSA] were found to be the best additives for the Cu/HfO$_2$/Pt cell in terms of a low switching voltage.

We further established a method that improves both the cyclic endurance and working voltage variability by the addition of a trace amount of Cu(Tf$_2$N)$_2$/[bmim][Tf$_2$N] to the HfO$_2$ film. Complex-impedance measurements suggest that there are two competing factors by the Cu doping; the decline in the Cu ion diffusion and the enhancement of the Cu ionization. The balance of these two factors determines the important parameters such as the cycling endurance, Vset, and its variability.

Therefore, the performance of the CB-RAM can be optimized by adjustment of the IL, considering the balance of the competing factors revealed by the present study, *i.e.*, σ_i, β, R_{sol}, and R_{ct}.
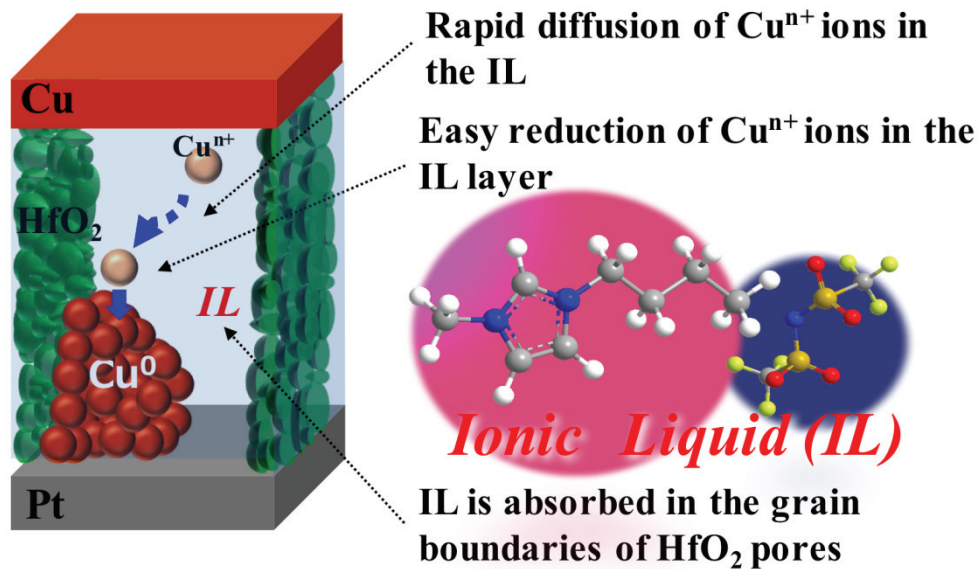
Figure 5-10. Plausible mechanism suggested by this study. The smooth formation of the Cu filament (set) is enhanced in the IL solution, whereas the rupture of the filament occurs due to thermal diffusion of the Cu atoms by Joule heating.

Chapter 6. Summery

We established that the IL remarkably improved the stability of the electrolyte of a CB-RAM ($Cu/HfO_2/Pt$) and reduced the operating voltage, and remarkable improvement of cycling endurance and working voltage variance has been achieved by addition of a trace amount of a $Cu(Tf_2N)_2/[bmim][Tf_2N]$ to the HfO_2 film layer of a CB-RAM with $Cu/HfO_2/Pt$ structure. And we also found that ionic conductivity of the IL and the coordinating ability of the anion in the IL towards the Cu ion are key competing factors that determine the voltage required for the formation of the Cu filament. The performance of the CB-RAM can be optimized by the adjustment of the IL, considering the balance of the competing factors revealed by the present study.

Chapter 7. Ionic liquid syntheses

General methods

The starting chemicals, solvents and materials for purification were purchased from suppliers shown in Figures 7-1, 7-2 and 7-3. In the case of some starting chemicals, we purified them prior to use as shown in the same figures. NMR spectra were recorded by Bruker AVANCE II 600 spectrometer (600 MHz for ^{1}H, 565 MHz for ^{19}F and 243 MHz for ^{31}P) instrument. The chemical shifts were reported in δ values relative to TMS (δ 0.0 ppm for ^{1}H) and C_6F_6 (δ 0.0 ppm for ^{19}F). Coupling constants (J) were reported in Hz. Water contents were measured by coulometric Karl Fischer titration using a Metrohm 831 KF Coulometer.

Table 7-1. Detail information of solvents

Material name	Supplier*	Purity	Note
Acetonitrile	Wako	>99.8%	dehydrated grade reagent
Dichloromethane	Wako	>99.0%	-
2-Propanol	Cica	>99.7%	-
Tetrahydrofuran (THF)	Wako	>99.5%	stabilizer free
Diethyl ether (Et$_2$O)	Cica	>99.5%	-
Acetone	Wako	>99.5%	dehydrated grade reagent
2-Butanol	Cica	>99.0%	-
Methanol	Cica	>99.7%	-
Ethyl acetate	Cica	>99.5%	-
Ethanol	Cica	>99.5%	-
N,N-dimethylformamide (DMF)	Cica	>99.5%	dehydrated grade reagent
tert-Butyl alcohol	TCI	>99.0%	-
CHCl$_3$	Wako	>99.0%	-

* TCI: Tokyo Chemical Industries Co., Ltd, Aldrich: Sigma-Aldrich,
   Wako: Wako Pure Chemical Industries, Ltd., Cica: KANTO CHEMICAL CO.,INC.

Table 7-2. Detail information of materials for purification

| Material name	Supplier*	Purity	Note
Activated carbon (granular)	Wako	-	-
Silica gel	Cica	-	60N soherical, neutral 63-210 mm
Alumina (neutral)	Aldrich	-	activated, neutral, Brockmann I
MgSO$_4$ (Anhydrous)	Wako	>98.0%	-

* TCI: Tokyo Chemical Industries Co., Ltd, Aldrich: Sigma-Aldrich,
   Wako: Wako Pure Chemical Industries, Ltd., Cica: KANTO CHEMICAL CO.,INC.

Table 7-3. Detail information of starting materials

| Material name	Supplier[*]	Purity	Note
1-Methylimidazole	TCI	>99.0%	distilled prior to use
1-Butylimidazole	TCI	>98.0%	distilled prior to use
1,2-Dimethylimidazole	Aldrich	>98%	recrystallized prior to use
1-Methylpiperidine	Cica	>98.0%	distilled prior to use
N,N-diethylmethylamine	Wako	>98.0%	distilled prior to use
4-Methylmorpholine	TCI	>99.0%	distilled prior to use
Pyridine	Wako	>99.5%	dehydrated grade reagent
1,2,4-Triazole	TCI	>99.0%	-
Bromoethane	TCI	>99.0%	-
1-Chlorobutane	TCI	>99.0%	-
1-Bromobutane	Aldrich	>99%	-
1-Iodobutane	TCI	>98.0%	-
1-Bromohexane	Aldrich	>98%	-
1-Bromooctane	Wako	>95.0%	-
2-Bromoethanol	Cica	>97.0%	-
2-(Methylthio)ethanol	TCI	>98.0%	-
2-Bromoethyl methyl ether	TCI	>95.0%	-
1-Methoxyethoxymethyl chloride	TCI	>95.0%	distilled prior to use
Iodomethane	Wako	>95.0%	-
Lithium bis(trifluoromethanesulfonyl)amide	TCI	>98.0%	-
Potassium bis(fluorosulfonyl)amide	Cica	>98.0%	-
48% HBF_4 aq.	Wako	>42.0%	-
Potassium hexafluorophosphate	TCI	>95.0%	-
Methyl trifluoromethanesulfonate	TCI	>98.0%	-
Methyl trifluoroacetate	TCI	>98.0%	-
Dimethyl sulfate	TCI	>98.0%	distilled prior to use
Trimethyl phosphate	TCI	>98.0%	-
Phosphorus tribromide	Wako	>90.0%	-
Tributylphosphine	TCI	>95.0%	distilled prior to use
Amberlite® IRN78 hydroxide form	Aldrich	-	washed and stored in de-ionized water prior to use
$AgNO_3$	Wako	>99.5%	-
$NaN(CN)_2$	TCI	>98.0%	-
Sodium azide	Wako	>98.0%	-
Copper (I) iodide	Wako	>95.0%	-
Trimethylsilylacetylene	TCI	>98.0%	-
Potassium *tert*-butoxide	Wako	>85.0%	-
Sodium methoxide (28% in MeOH)	Wako	(27-29%)	-
Tf_2NH	Cica	>98.0%	-
CuO (powder, 3N)	Cica	>99.9%	-
1-(2-Pyridylazo)-2-naphthol (PAN)	TCI	>98.0%	-
Ethylenediaminetetraacetic acid disodium salt dihydrate (EDTA disodium salt dihydrate)	Wako	>99.5%	-

* TCI: Tokyo Chemical Industries Co., Ltd, Aldrich: Sigma-Aldrich,
  Wako: Wako Pure Chemical Industries, Ltd., Cica: KANTO CHEMICAL CO.,INC.

1-Ethyl-3-methylimidazolium bis(trifluoromethanesulfonyl)amide ([emim][Tf₂N])[49]
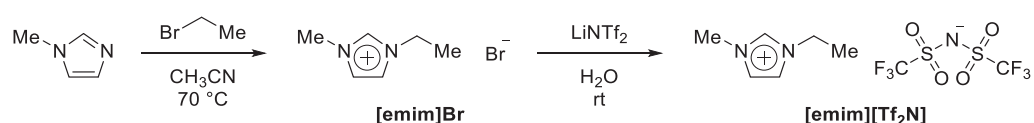
Under argon atmosphere, a 1.5 equiv. amount of bromoethane (17 mL) was added to a solution of 1-methylimidazole (12.3 g, 150 mmol) and dry acetonitrile (CH₃CN) (30 mL). The reaction mixture was stirred at 70 °C for overnight and cooled to room temperature. The solvent was removed under reduced pressure and then, concentrated *in vacuo* (*ca.* 100 Pa, 70 °C). The residual white solid was purified by recrystallization from 2-propanol/ tetrahydrofuran (THF) (30 mL/100 mL) to give [emim]Br (27.0 g, 94% yield). This was used for the next reaction without further purification. An aqueous solution of [emim]Br (5.7 g, 30 mmol) in de-ionized water (10 mL) was mixed with an aqueous solution of lithium bis(trifluoromethanesulfonyl)amide (8.6 g) in 15 mL of de-ionized water at room temperature (rt) then the mixture was stirred at rt for 12 h. The resulting mixture was diluted with 10 mL of dichloromethane and the organic layer was separated by decantation. The residual water layer was extracted by dichloromethane (15 mL) twice, and the combined organic layers were washed with de-ionized water (30 mL) four times until Br⁻ didn't detected using AgNO₃ aq. solution. The solvent was removed under reduced pressure and dried *in vacuo* (<100 Pa, 70 °C) to give [emim][Tf₂N]: colorless liquid. ¹H NMR (600 MHz, acetone-d₆) δ 1.57 (3H, t, *J* = 7.2), 4.05 (3H, s), 4.39 (2H, q, *J* = 7.2), 7.68 (1H, s), 7.75 (1H, s), 8.98 (1H, s); ¹⁹F NMR (565 MHz, acetone-d6) δ 84.7 (6F, s); Water content: 116 ppm, [emim]Br: ¹H NMR (600 MHz, CDCl₃) δ 1.62 (3H, t, *J* = 7.2), 4.14 (3H, s), 4.45 (2H, q, *J* = 7.2), 7.73 (1H, s), 7.73 (1H, s), 10.28 (1H, s).

1-Butyl-3-methylimidazolium bis(trifluoromethanesulfonyl)amide ([bmim][Tf₂N])[50]
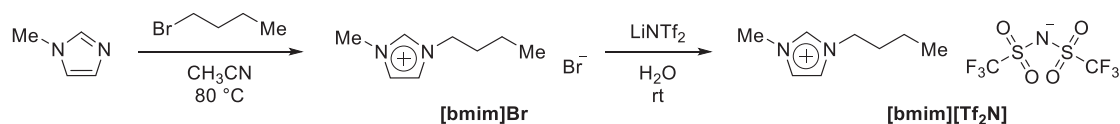
Under argon atmosphere, a 1.0 equiv. amount of 1-bromobutane (17 mL) was added to a solution of 1-methylimidazole (12.3 g, 150 mmol) and dry CH₃CN (30 mL). The reaction mixture was stirred at 80 °C for overnight and cooled to room temperature. The solvent was removed under reduced pressure and then, concentrated *in vacuo* (*ca.* 100 Pa, 50 °C). The residual white solid was purified by recrystallization from 2-propanol/THF (40 mL/390 mL) to give [bmim]Br (28.8 g, 88% yield). This was used for the next reaction without further purification. An aqueous solution of [bmim]Br (28.8 g, 131 mmol) in

de-ionized water (40 mL) was mixed with an aqueous solution of lithium bis(trifluoromethanesulfonyl)amide (37.7 g) in 60 mL of de-ionized water at room rt then the mixture was stirred at rt for 12 h. The resulting mixture was diluted with 20 mL of dichloromethane and the organic layer was separated by decantation. The residual water layer was extracted by dichloromethane (60 mL) twice, and the combined organic layers were washed with de-ionized water (120 mL) four times until Br$^-$ didn't detected using AgNO$_3$ aq. solution. The solvent was removed under reduced pressure and dried *in vacuo* (<100 Pa, 80 °C) to give [bmim][Tf$_2$N] (53.3 g, 97% yield): colorless liquid. ^{1}H NMR (600 MHz, acetone-d$_6$) δ 0.95 (3H, t, J = 7.2), 1.39 (2H, sext, J = 7.2), 1.94 (2H, quint, J = 7.2), 4.08 (3H, s), 4.38 (2H, t, J = 7.2), 7.72-7.73 (1H, m), 7.78-7.79 (1H, m), 9.05 (1H, s) ; ^{19}F NMR (565 MHz, acetone-d$_6$) δ 84.7 (6F, s); Water content: 125 ppm, [bmim]Br: ^{1}H NMR (600 MHz, CDCl$_3$) δ 0.97 (3H, t, J = 7.2), 1.39 (2H, sext, J = 7.2), 1.92 (2H, quint, J = 7.2), 4.15 (3H, s), 4.36 (2H, t, J = 7.2), 7.48-7.49 (1H, m), 7.60-7.61 (1H, m), 10.35 (1H, s).
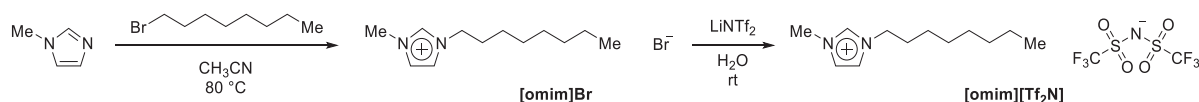
1-Hexyl-3-methylimidazolium bis(trifluoromethanesulfonyl)amide ([hmim][Tf$_2$N]) [51]
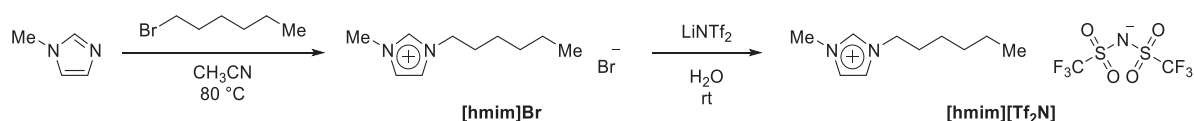
Under argon atmosphere, a 1.0 equiv. amount of 1-bromohexane (14 mL) was added to a solution of 1-methylimidazole (8.2 g, 100 mmol) and dry CH$_3$CN (20 mL). The reaction mixture was stirred at 80 °C for overnight and cooled to room temperature. The solvent was removed under reduced pressure and then, concentrated *in vacuo* (*ca.* 100 Pa, 70 °C). The residual oil was dissolved in CH$_3$CN (20 mL), and washed with Et$_2$O (60 mL). After removal of Et$_2$O layer, activated carbon (granular, 1g) was added to residual solution. The filtrate was concentrated under reduced pressure and dried *in vacuo* to give [hmim]Br (23.7 g, 96% yield). This was used for the next reaction without further purification. An aqueous solution of [hmim]Br (7.4 g, 30 mmol) in de-ionized water (10 mL) was mixed with an aqueous solution of lithium bis(trifluoromethanesulfonyl)amide (8.6 g) in 15 mL of de-ionized water at room rt then the mixture was stirred at rt for 12 h. The resulting mixture was diluted with 10 ml of dichloromethane and the organic layer was separated by decantation. The residual water layer was extracted by dichloromethane (15 mL) twice, and the combined organic layers were washed with de-ionized water (30 mL) three times until Br$^-$ didn't detected using AgNO$_3$ aq. solution. The solvent was removed under reduced pressure and dried *in vacuo* (<100 Pa, 70 °C) to give [hmim][Tf$_2$N] (13.1 g, 98% yield): colorless liquid. ^{1}H NMR (600 MHz, acetone-d$_6$) δ 0.87 (3H, t, J = 7.2), 1.29-1.41 (6H, m), 1.95 (2H, quint, J = 7.2), 4.07 (3H, s), 4.38 (2H, t, J = 7.2), 7.72-7.73 (1H, m), 7.78-7.79 (1H, m), 9.04 (1H, s); ^{19}F NMR (565 MHz, acetone-d$_6$) δ 84.7 (6F,

s); Water content: 85 ppm, [hmim]Br: ^{1}H NMR (600 MHz, CDCl$_3$) δ 0.87 (3H, t, J = 7.2), 1.28-1.38 (6H, m), 1.93 (2H, quint, J = 7.2), 4.15 (3H, s), 4.35 (2H, t, J = 7.2), 7.59-7.60 (1H, m), 7.77-7.78 (1H, m), 10.33 (1H, s).

1-Methyl-3-octylimidazolium bis(trifluoromethanesulfonyl)amide ([omim][Tf$_2$N])[51]

Under argon atmosphere, a 1.0 equiv. amount of 1-bromooctane (17.4 mL) was added to a solution of 1-methylimidazole (8.2 g, 100 mmol) and dry CH$_3$CN (20 mL). The reaction mixture was stirred at 80 °C for overnight and cooled to room temperature. The solution was washed with Et$_2$O (60 mL), and the Et$_2$O layer was removed. Then, activated carbon (granular, 1g) was added to residual solution. The filtrate was concentrated under reduced pressure and dried *in vacuo* to give [omim]Br (26.7 g, 97% yield). This was used for the next reaction without further purification. An aqueous solution of [omim]Br (8.3 g, 30 mmol) in de-ionized water (10 mL) was mixed with an aqueous solution of lithium bis(trifluoromethanesulfonyl)amide (8.6 g) in 15 mL of de-ionized water at room rt then the mixture was stirred at rt for 12 h. The resulting mixture was diluted with 15 mL of dichloromethane and the organic layer was separated by decantation. The residual water layer was extracted by dichloromethane (15 mL) twice, and the combined organic layers were washed with de-ionized water (30 mL) three times until Br$^-$ didn't detected using AgNO$_3$ aq. solution. The solvent was removed under reduced pressure and dried *in vacuo* (<100 Pa, 70 °C) to give [omim][Tf$_2$N] (13.9 g, 98% yield): colorless liquid. ^{1}H NMR (600 MHz, acetone-d$_6$) δ 0.87 (3H, t, J = 7.2), 1.24-1.40 (10H, m), 1.96 (2H, quint, J = 7.2), 4.06 (3H, s), 4.37 (2H, t, J = 7.2), 7.71-7.72 (1H, m), 7.77-7.78 (1H, m), 9.03 (1H, s); ^{19}F NMR (565 MHz, acetone-d$_6$) δ 84.7 (6F, s); Water content: 92 ppm, [omim]Br: ^{1}H NMR (600 MHz, CDCl$_3$) δ 0.87 (3H, t, J = 7.8), 1.25-1.39 (10H, m), 1.97 (2H, quint, J = 7.8), 4.15 (3H, s), 4.50 (2H, t, J = 7.8), 8.05-8.06 (1H, m), 8.14-8.15 (1H, m), 10.31 (1H, s).

1-Butyl-2, 3-dimethylimidazolium bis(trifluoromethanesulfonyl)amide ([bdmim][Tf$_2$N])[50]
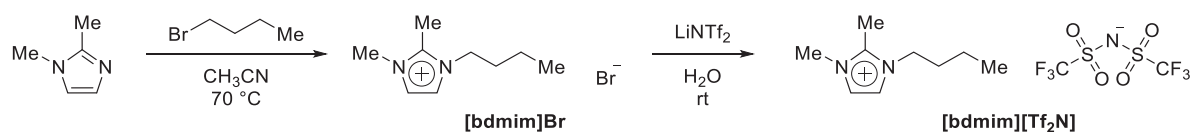
Under argon atmosphere, a 1.1 equiv. amount of 1-bromobutane (15 mL) was added to a solution of 1, 2-dimethylimidazole (9.6 g, 100 mmol) and dry CH$_3$CN (20 mL). The reaction mixture was stirred at 70 °C for overnight and cooled to room temperature. The solvent was removed under reduced pressure and then, concentrated *in vacuo*. The residual solid was purified by recrystallization from 2-propanol/THF (25 mL/140 mL) twice to give [bdmim]Br (19.5 g, 84% yield). This was used for the next reaction without further purification. An aqueous solution of [bdmim]Br (7.0 g, 30 mmol) in de-ionized water (10 mL) was mixed with an aqueous solution of lithium bis(trifluoromethanesulfonyl)amide (8.6 g) in 15 mL of de-ionized water at room rt then the mixture was stirred at rt for 12 h. The resulting mixture was diluted with 15 mL of dichloromethane and the organic layer was separated by decantation. The residual water layer was extracted by dichloromethane (15 mL) twice, and the combined organic layers were washed with de-ionized water (30 mL) three times until Br⁻ didn't detected using AgNO$_3$ aq. solution. The solvent was removed under reduced pressure, and dried *in vacuo* (<100 Pa, 70 °C). The product was dissolved in dichloromethane (50 mL) and treated with an activated carbon (granular, 1 g). The solvent of the filtrate was removed and dried *in vacuo* (<100 Pa, 70 °C) again to give [bdmim][Tf$_2$N] (12.8 g, 98% yield): colorless liquid. ^{1}H NMR (600 MHz, acetone-d$_6$) δ 0.97 (3H, t, *J* = 7.8), 1.42 (2H, sext, *J* = 7.8), 1.87 (2H, quint, *J* = 7.8), 2.79 (3H, s), 3.96 (3H, s), 4.30 (2H, t, *J* = 7.8), 7.60 (1H, d, *J* = 1.8), 7.64 (1H, d, *J* = 1.8); ^{19}F NMR (565 MHz, acetone-d$_6$) δ 84.7 (6F, s); Water content: 32 ppm, [bdmim]Br: ^{1}H NMR (600 MHz, CDCl$_3$) δ 0.96 (3H, t, *J* = 7.8), 1.41 (2H, sext, *J* = 7.8), 1.82 (2H, quint, *J* = 7.8), 2.85 (3H, s), 4.06 (3H, s), 4.27 (2H, t, *J* = 7.8), 7.62 (1H, d, *J* = 1.8), 7.81 (1H, d, *J* = 1.8).


1-Methoxyethyl-3-methylimidazolium bis(trifluoromethanesulfonyl)amide ([MEmim][Tf$_2$N])[52]

Under argon atmosphere, a 1.0 equiv. amount of 2-bromoethyl methyl ether (14 mL) was added to a solution of 1-methylimidazole (8.2 g, 100 mmol) and dry CH$_3$CN (25 mL). The reaction mixture was stirred at 80 °C for overnight and cooled to room temperature. The solvent was removed under reduced pressure

and then, concentrated *in vacuo*. The residual solid was purified by recrystallization from 2-propanol/THF (60 mL/300 mL) to give [MEmim]Br (19.6 g, 89% yield). This was used for the next reaction without further purification. An aqueous solution of [MEmim]Br (6.6 g, 30 mmol) in de-ionized water (10 mL) was mixed with an aqueous solution of lithium bis(trifluoromethanesulfonyl)amide (8.6 g) in 15 mL of de-ionized water at room rt then the mixture was stirred at rt for 12 h. The resulting mixture was diluted with 15 mL of dichloromethane and the organic layer was separated by decantation. The residual water layer was extracted by dichloromethane (15 mL) twice, and the combined organic layers were washed with de-ionized water (30 mL) three times until Br$^-$ didn't detected using AgNO$_3$ aq. solution. The solvent was removed under reduced pressure and dried *in vacuo* (<100 Pa, 70 °C) to give [MEmim][Tf$_2$N] (12.1 g, 96% yield): colorless liquid. ^{1}H NMR (600 MHz, acetone-d$_6$) ^{1}H NMR (600 MHz, CDCl$_3$) δ 3.35 (3H, s), 3.81 (2H, t, J = 4.8), 4.08 (3H, s), 4.53 (2H, t, J = 4.8), 7.69-7.70 (1H, m), 7.73-7.74 (1H, m), 9.00 (1H, s); ^{19}F NMR (565 MHz, acetone-d$_6$) δ 84.7 (6F, s); Water content: 88 ppm, [MEmim]Br: ^{1}H NMR (600 MHz, CDCl$_3$) δ 3.38 (3H, s), 3.79 (2H, t, J = 7.2), 4.13 (3H, s), 4.60 (2H, t, J = 7.2), 7.67-7.69 (2H, m), 10.10 (1H, s).

1-Butyl-3-methyl-1, 2, 3-triazolium bis(trifluoromethanesulfonyl)amide ([bmtr][Tf$_2$N])[53,54]
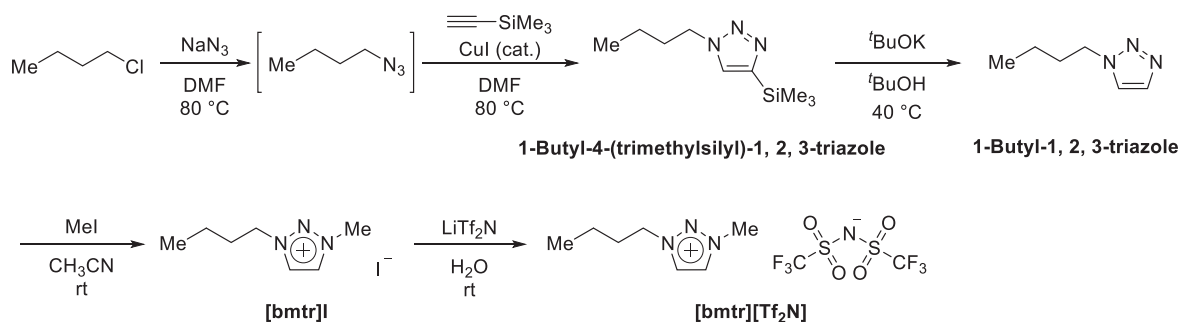

Under argon atmosphere, 1-chlorobutane (2.78 g, 30 mmol) was added to a suspension of sodium azide (5.1 g, 2.6 eq.) and 38 mL of dry *N,N*-dimethylformamide (DMF). The reaction mixture was stirred at 80 °C for overnight and cooled to room temperature. Then, copper (I) iodide (0.76 g, 13 mol%) and trimethylsilylacetylene (5.4 mL, 1.3 eq.) were added, and the mixture was stirred at 80 °C again for overnight and cooled to room temperature. The precipitate was filtered off, and the filtrate was concentrated under reduced pressure. The obtained oil was purified by column chromatography on silica gel (hexane/AcOEt = 5/1) to give 1-butyl-4-(trimethylsilyl)-1, 2, 3-triazole (3.8 g, 65% yield).

Potassium *tert*-butoxide (2.33 g, 1.5 eq.) was added to a solution of 1-butyl-4-(trimethylsilyl)-1, 2, 3-triazole (2.74 g, 13.9 mmol) and ^{t}BuOH (28 mL). The reaction mixture was stirred at 40 °C for overnight and cooled to room temperature. Then, H$_2$O (56 mL) was added to the mixture, and extracted by

Et$_2$O (90 mL) five times. The combined organic layer was dried over MgSO$_4$, and concentrated under reduced pressure to give 1-butyl-1, 2, 3-triazole (1.64 g, 88% yield).

Under argon atmosphere, a 1.05 equiv. amount of iodomethane (1.6 mL) was added to a solution of 1-butyl-1, 2, 3-triazole (1.62 g, 12.9 mmol) and dry CH$_3$CN (2 mL) at 0 °C. The reaction mixture was stirred at 0 °C for 1 h, then warmed to room temperature and stirred in the dark for 7 days. The solvent was removed under reduced pressure and dried *in vacuo* to give [bmtr]I (3.34 g, 97% yield). This was used for the next reaction without further purification. An aqueous solution of [bmtr]I (3.33 g, 12.5 mmol) in de-ionized water (5 mL) was mixed with an aqueous solution of lithium bis(trifluoromethanesulfonyl)amide (3.58 g) in 8 mL of de-ionized water at room rt then the mixture was stirred at rt for 12 h. The resulting mixture was diluted with 10 mL of dichloromethane and the organic layer was separated by decantation. The residual water layer was extracted by dichloromethane (10 mL) twice, and the combined organic layers were washed with de-ionized water (20 mL) three times until Br$^-$ didn't detected using AgNO$_3$ aq. solution. The solvent was removed under reduced pressure, and the obtained oil was treated with activated carbon (granular, 3 g) in methanol (50 mL) and the filtrate was concentrated again. The oil was passed through alumina column (neutral Al$_2$O$_3$ 10 g, eluent: acetone). The filtrate was concentrated under reduced pressure, and dried *in vacuo* (<100 Pa, 50 °C) to give [bmtr][Tf$_2$N] (3.64 g, 70% yield): colorless liquid. ^{1}H NMR (600 MHz, acetone-d$_6$) δ 0.97 (3H, t, J = 7.2), 1.43 (2H, sext, J = 7.2), 2.06 (2H, quint, J = 7.2), 4.52 (3H, s), 4.80 (2H, t, J = 7.2), 8.81 (1H, d, J = 1.2), 8.85 (1H, d, J = 1.2); ^{19}F NMR (565 MHz, acetone-d$_6$) δ 84.7 (6F, s); Water content: 46 ppm, 1-Butyl-4-(trimethylsilyl)-1, 2, 3-triazole: ^{1}H NMR (600 MHz, CDCl$_3$) δ 0.32 (9H, s), 0.96 (3H, t, J = 7.2), 1.37 (2H, sext, J = 7.2), 1.89 (2H, quint, J = 7.2), 4.38 (2H, t, J = 7.2), 7.50 (1H, s), 1-butyl-1, 2, 3-triazole: ^{1}H NMR (600 MHz, CDCl$_3$) δ 0.96 (3H, t, J = 7.2), 1.36 (2H, sext, J = 7.2), 1.90 (2H, quint, J = 7.2), 4.40 (2H, t, J = 7.2), 7.56 (1H, s), 7.70 (1H, s), [bmtr]I: ^{1}H NMR (600 MHz, CDCl$_3$) δ 0.99 (3H, t, J = 7.2), 1.44 (2H, sext, J = 7.2), 2.05 (2H, quint, J = 7.2), 4.56 (3H, s), 4.79 (2H, t, J = 7.2), 9.42 (1H, d, J = 1.2), 9.46 (1H, d, J = 1.2).

N-Butyl-*N*, *N*-diethyl-*N*-methylammonium bis(trifluoromethanesulfonyl)amide ([N$_{1224}$][Tf$_2$N])[55,56]
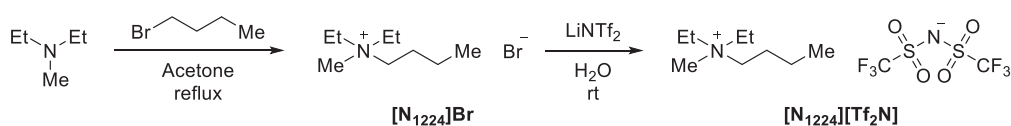
Under argon atmosphere, a 1.0 equiv. amount of 1-bromobutane (11 mL) was added to a solution of *N*, *N*-diethylmethylamine (8.7 g, 100 mmol) and dry acetone (27 mL). The reaction mixture was stirred with reflux (65 °C) for overnight and cooled to room temperature. The solvent was removed by filtration and

the obtained solid was washed with acetone. The filtrate was concentrated under reduced pressure and the obtained solid was purified by recrystallization from 2-propanol/THF (20 mL/380 mL) to give white solid. These obtained solids were dried *in vacuo* to give [N$_{1224}$]Br (17.4 g, 78% yield). This was used for the next reaction without further purification. An aqueous solution of [N$_{1224}$]Br (17.4 g, 77.5 mmol) in de-ionized water (25 mL) was mixed with an aqueous solution of lithium bis(trifluoromethanesulfonyl)amide (22.3 g) in 35 mL of de-ionized water at room rt then the mixture was stirred at rt for 12 h. The resulting mixture was diluted with 40 mL of dichloromethane and the organic layer was separated by decantation. The residual water layer was extracted by dichloromethane (40 mL) twice, and the combined organic layers were washed with de-ionized water (80 mL) three times until Br$^-$ didn't detected using AgNO$_3$ aq. solution. The solvent was removed under reduced pressure and dried *in vacuo* (<100 Pa, 80 °C) to give [N$_{1224}$][Tf$_2$N] (32.1 g, 98% yield): colorless liquid. ^{1}H NMR (600 MHz, acetone-d$_6$) δ 0.99 (3H, t, *J* = 7.2), 1.40-1.46 (8H, m), 1.81-1.83 (2H, m), 3.14 (3H, s), 3.38-3.41 (2H, m), 3.52 (4H, q, *J* = 7.2); ^{19}F NMR (565 MHz, acetone-d$_6$) δ 84.8 (6F, s); Water content: 36 ppm, [N$_{1224}$]Br: ^{1}H NMR (600 MHz, CDCl$_3$) δ 1.01 (3H, t, *J* = 7.2), 1.41 (6H, t, *J* = 7.2), 1.45 (2H, sext, *J* = 7.2), 1.69-1.75 (2H, m), 3.28 (3H, s), 3.44-3.47 (2H, m), 3.64 (4H, q, *J* = 7.2).

1-Butyl-1-methypiperidinium bis(trifluoromethanesulfonyl)amide ([PP$_{14}$][Tf$_2$N])[57]
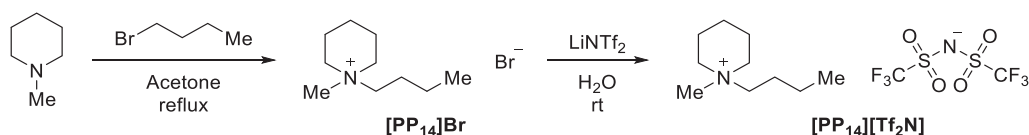
Under argon atmosphere, a 1.0 equiv. amount of 1-bromobutane (3.2 mL) was added to a solution of 1-methylpiperidine (3.0 g, 30 mmol) and dry acetone (8 mL). The reaction mixture was stirred with reflux (65 °C) for overnight and cooled to room temperature. The solvent was removed by filtration and the ob-tained solid was washed with Et$_2$O (15 mL) three times. The solid was purified by recrystallization from 2-propanol/THF (20 mL/30 mL) to give [PP$_{14}$]Br (4.4 g, 63% yield). This was used for the next reaction without further purification. An aqueous solution of [PP$_{14}$]Br (2.4 g, 10 mmol) in de-ionized water (3 mL) was mixed with an aqueous solution of lithium bis(trifluoromethanesulfonyl)amide (2.9 g) in 8 mL of de-ionized water at room rt then the mixture was stirred at rt for 12 h. The resulting mixture was diluted with 5 mL of dichloromethane and the organic layer was separated by decantation. The residual water layer was extracted by dichloromethane (5 mL) twice, and the combined organic layers were washed with de-ionized water (20 mL) three times until Br$^-$ didn't detected using AgNO$_3$ aq. solution. The solvent was removed under reduced pressure and dried *in vacuo* (<100 Pa, 70 °C) to give [PP$_{14}$][Tf$_2$N] (4.1 g, 93% yield): colorless liquid. ^{1}H NMR (600 MHz, CDCl$_3$) δ 0.99 (3H, t, *J* = 7.2), 1.42 (2H, quint, *J* = 7.2),

1.68-1.89 (8H, m), 3.02 (3H, s), 3.26-3.35 (6H, m); ^{19}F NMR (565 MHz, CDCl$_3$) δ 84.8 (6F, s); Water content: 50 ppm, [PP$_{14}$]Br: ^{1}H NMR (600 MHz, CDCl$_3$) δ 1.00 (3H, t, J = 7.2), 1.46 (2H, sext, J = 7.2), 1.81-1.96 (8H, m), 3.34 (3H, s), 3.66-3.71 (4H, m), 3.74-3.78 (2H, m).

1-Butylpyridinium bis(trifluoromethanesulfonyl)amide ([Py$_4$][Tf$_2$N])[58,59]


[Py$_4$]Br   **[Py$_4$][Tf$_2$N]**
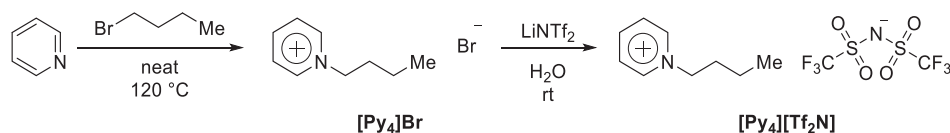
Under argon atmosphere, a 1.1 equiv. amount of 1-bromobutane (18 mL) was added to pyridine (11.9 g, 150 mmol). The reaction mixture was stirred with reflux (120 °C) for overnight and cooled to room temperature. The residual reagent was removed under reduced pressure, and obtained solid was purified by recrystallization from 2-propanol/THF (50 mL/330 mL) to give [Py$_4$]Br (29.1 g, 90% yield). This was used for the next reaction without further purification. An aqueous solution of [Py$_4$]Br (13.0 g, 60 mmol) in de-ionized water (20 mL) was mixed with an aqueous solution of lithium bis(trifluoromethanesulfonyl)amide (17.2 g) in 30 mL of de-ionized water at room rt then the mixture was stirred at rt for 12 h. The resulting mixture was diluted with 30 mL of dichloromethane and the organic layer was separated by decantation. The residual water layer was extracted by dichloromethane (30 mL) twice, and the combined organic layers were washed with de-ionized water (60 mL) three times until Br$^-$ didn't detected using AgNO$_3$ aq. solution. The solvent was removed under reduced pressure and dried *in vacuo* (<100 Pa, 80 °C) to give [Py$_4$][Tf$_2$N] (24.3 g, 97% yield): colorless liquid. ^{1}H NMR (600 MHz, acetone-d$_6$) δ 0.99 (3H, t, J = 7.2), 1.46 (2H, sext, J = 7.2), 2.11 (2H, quint, J = 7.2), 4.85 (2H. t, J = 7.2), 8.27-8.28 (2H, m), 8.73-8.75 (1H, m), 9.17 (2H, d, J = 6.0); ^{19}F NMR (565 MHz, acetone-d$_6$) δ 84.7 (6F, s); Water content: 65 ppm, [Py$_4$]Br: ^{1}H NMR (600 MHz, CDCl$_3$) δ 0.97 (3H, t, J = 7.2), 1.44 (2H, sext, J = 7.2), 2.07 (2H, quint, J = 7.2), 5.04 (2H. t, J = 7.2), 8.19-8.21 (2H, m), 8.58-8.60 (1H, m), 9.67 (2H, d, J = 5.3).

1-Butyl-3-methylimidazolium bis(fluorosulfonyl)amide ([bmim][FSA])[60]
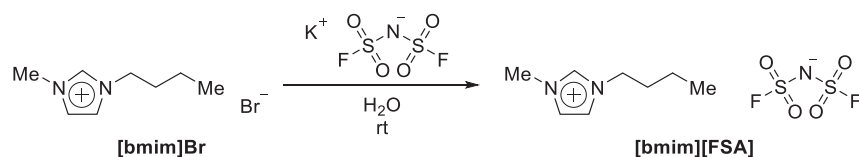
An aqueous solution of [bmim]Br (6.6 g, 30 mmol) in de-ionized water (10 mL) was mixed with an aqueous solution of potassium bis(fluorosulfonyl)amide (6.6 g) in 15 mL of de-ionized water at room rt then the mixture was stirred at rt for 12 h. The resulting mixture was diluted with 15 mL of dichloromethane and the organic layer was separated by decantation. The residual water layer was extracted by dichloromethane (15 mL) twice, and the combined organic layers were washed with de-ionized water (30 mL) three times until Br$^-$ didn't detected using AgNO$_3$ aq. solution. The solvent was removed under reduced pressure and dried *in vacuo* (<100 Pa, 70 °C) to give [bmim][FSA] (9.2 g, 95% yield): colorless liquid. ^{1}H NMR (600 MHz, acetone-d$_6$) δ 0.96 (3H, t, *J* = 7.2), 1.40 (2H, sext, *J* = 7.2), 1.94 (2H, quint, *J* = 7.2), 4.06 (3H, s), 4.36 (2H, t, *J* = 7.2), 7.69, (1H, s), 7.75 (1H, s), 8.99 (1H, s) ; ^{19}F NMR (565 MHz, acetone-d$_6$) δ 216.1 (2F, s); Water content: 104 ppm.

1-Butyl-3-methylimidazolium tetrafluoroborate ([bmim][BF$_4$])[61]
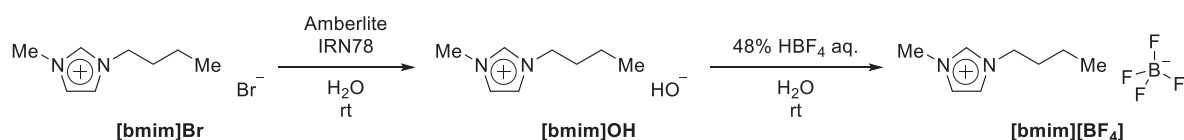
Amberlite IRN78 (30 mL) was added to a solution of [bmim]Br (4.4 g, 20 mmol) and de-ionized water (130 mL). The reaction mixture was stirred at room temperature for a week until AgNO$_3$ aq. check turned negative. The Amberlite was removed by filtration to give aqueous solution of [bmim]OH (224 g, 0.09 mmol/g). This solution was used for the next reaction without further purification. A mixture of 48% HBF$_4$ aq. (3.7 g) and de-ionized water (20 mL) was added to [bmim]OH aq. (224g, 20 mmol) until pH of the reaction mixture turned *ca.* 4 at 0 °C. The solvent was removed under reduced pressure, and the residual oil was passed through alumina column (neutral Al$_2$O$_3$ 10 g, eluent: dichloromethane). The obtained solution was concentrated under reduced pressure, and treated with activated carbon (powder, 2.5 g) in methanol (100 mL). The filtrate was concentrated under reduced pressure and dried *in vacuo* (<100 Pa, 50 °C) to give [bmim][BF$_4$] (3.4 g, 75% yield): pale yellow liquid. ^{1}H NMR (600 MHz, CDCl$_3$) δ 1.01 (3H, t, *J* = 7.2), 1.40 (2H, sext, *J* = 7.2), 1.90 (2H, quint, *J* = 7.2), 3.95 (3H, s), 4.24 (2H, t, *J* = 7.2),

7.58 (1H, d, $J = 1.8$), 7.64 (1H, d, $J = 1.8$), 8.90 (1H, s) ; ^{19}F NMR (565 MHz, CDCl$_3$) δ 11.3 (4F, d, $J = 28.3$); Water content: 2602 ppm, aqueous solution of [bmim]OH: ^{1}H NMR (600 MHz, D$_2$O) δ 0.78 (3H, t, $J = 7.2$), 1.17 (2H, sext, $J = 7.2$), 1.69 (2H, quint, $J = 7.2$), 4.05 (3H, s), 3.74 (2H, t, $J = 7.2$), 7.28 (1H, d, $J = 1.5$), 7.32 (1H, d, $J = 1.5$), 8.56 (1H, br).

1-Butyl-3-methylimidazolium hexafluorophosphate ([bmim][PF$_6$])[62]
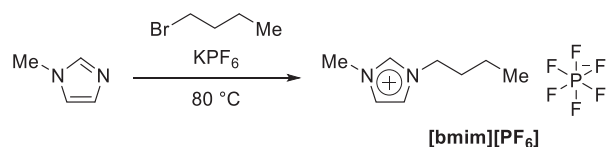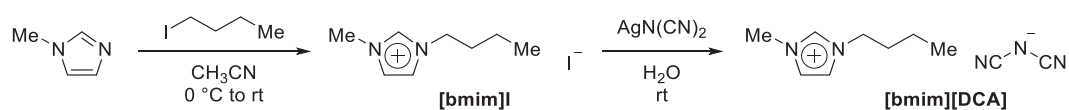

A mixture of 1-methylimidazole (4.1 g, 50 mmol), 1-bromobutane (6.9 g, 1.0 eq.) and potassium hexafluorophosphate (9.2 g, 1.0 eq.) was stirred at 80 °C for 5 h, and cooled to room temperature. De-ionized water (20 mL) and dichloromethane (15 mL) were added to the reaction mixture, and stirred for 1 h. The organic layer was separated by decantation, and washed by de-ionized water (50 mL) five times until Br$^-$ didn't detected using AgNO$_3$ aq. solution. The solvent was removed under reduced pressure, and dried *in vacuo* (<100 Pa, 70 °C) to give [bmim][PF$_6$] (11.0 g, 78% yield): colorless liquid. ^{1}H NMR (600 MHz, acetone-d$_6$) δ 0.95 (3H, t, $J = 7.8$), 1.39 (2H, sext, $J = 7.8$), 1.93 (2H, quint, $J = 7.8$), 4.03 (3H, s), 4.34 (2H, t, $J = 7.8$), 7.67 (1H, d, $J = 1.8$), 7.73 (1H, d, $J = 1.8$), 8.90 (1H, s) ; ^{19}F NMR (565 MHz, acetone-d$_6$) δ 92.4 (6F, d, $J = 708$); ^{31}P NMR (243 MHz, acetone-d$_6$) δ -144.3 (6F, sept, $J = 708$); Water content: 173 ppm.
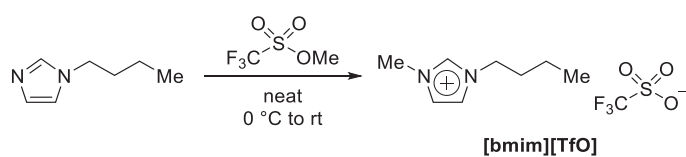
Silver (I) dicyanamide (AgN(CN)$_2$)[63]
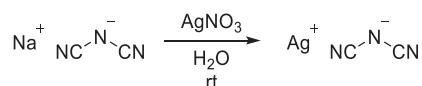
An aqueous solution of AgNO$_3$ (17.0 g in 50 mL of de-ionized water) was added to a solution of NaN(CN)$_2$ (8.9 g, 100 mmol) and de-ionized water (100 mL) dropwise. The reaction mixture was stirred at room temperature in the dark for overnight. The solvent was removed by filtration using membrane filter (0.45 μm). The obtained cake was washed with de-ionized water and acetone, and dried *in vacuo* to give AgN(CN)$_2$ as white solid (16.4 g, 95% yield).

1-Butyl-3-methylimidazolium dicyanamide ([bmim][DCA])[64,65]

Me—N⌒N $\xrightarrow[\text{0 °C to rt}]{\text{I}\diagdown\diagup\text{Me} \atop \text{CH}_3\text{CN}}$ Me—N⊕⌒N⌒⌒Me I⁻ **[bmim]I** $\xrightarrow[\text{rt}]{\text{AgN(CN)}_2 \atop \text{H}_2\text{O}}$ Me—N⊕⌒N⌒⌒Me NC–N⁻–CN **[bmim][DCA]**
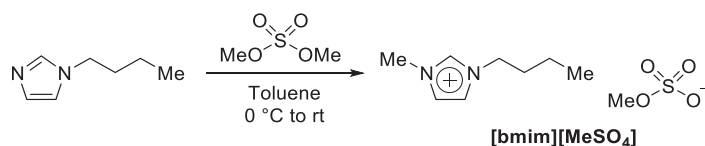
Under argon atmosphere, a 1.05 equiv. amount of 1-iodobutane (12 mL) was added to a solution of 1-methylimidazole (8.2 g, 100 mmol) and dry CH_3CN (15 mL) at 0 °C. The reaction mixture was stirred at 0 °C for 4 h, then warmed to room temperature and stirred in the dark for 8 days. The solvent was removed under reduced pressure and dried *in vacuo*. The residual oil was washed with AcOEt (30 mL) and Et_2O (30 mL), and dried in vacuo again to give [bmim]I (25.7 g, 96% yield). This was used for the next reaction without further purification. An aqueous solution of [bmim]I (16.0 g, 60 mmol in 200 mL of de-ionized water) was added to a suspension of $AgN(CN)_2$ (12.2 g, 1.2 eq.) and de-ionized water (400 mL) dropwise. The reaction mixture was stirred at room temperature in the dark for overnight. The precipitate was removed by filtration using membrane filter (0.45 μm). The obtained filtrate was concentrated under reduced pressure, and dried *in vacuo* (<100 Pa, rt) to give [bmim][DCA] (12.5 g, quantitative yield): colorless liquid. ^{1}H NMR (600 MHz, CD_3OD) δ 0.99 (3H, t, J = 7.8), 1.38 (2H, sext, J = 7.8), 1.87 (2H, quint, J = 7.8), 3.92 (3H, s), 4.21 (2H, t, J = 7.8), 7.56 (1H, s), 7.63 (1H, s), 8.91 (1H, s); Water content: 978 ppm, [bmim]I: ^{1}H NMR (600 MHz, $CDCl_3$) δ 0.98 (3H, t, J = 7.8), 1.41 (2H, sext, J = 7.8), 1.94 (2H, quint, J = 7.8), 4.14 (3H, s), 4.36 (2H, t, J = 7.8), 7.56-3.57 (1H, m), 7.64-7.65 (1H, m), 9.97 (1H, s).

1-Butyl-3-methylimidazolium trifluoromethanesulfonate ([bmim][TfO])[66]

N⌒N⌒⌒Me $\xrightarrow[\text{0 °C to rt}]{\text{F}_3\text{C–SO}_2\text{–OMe} \atop \text{neat}}$ Me—N⊕⌒N⌒⌒Me F_3C–SO$_2$–O⁻ **[bmim][TfO]**
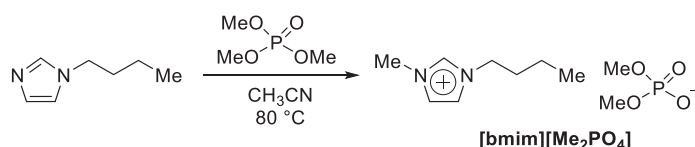
Under argon atmosphere, a 1.02 equiv. amount of methyl trifluoromethanesulfonate (2.51 g) was added to 1-butylimidazole (1.86 g, 15 mmol) at 0 °C. The reaction mixture was stirred at 0 °C for 5 h, then warmed to room temperature and stirred for overnight. The residual reagent removed *in vacuo*. The product was dissolved in methanol (50 mL) and treated with an activated carbon (granular, 3 g). The solvent of the filtrate was removed under reduced pressure, and dried *in vacuo* (<100 Pa, rt) to give [bmim][TfO] (3.53 g, 82% yield): colorless liquid. ^{1}H NMR (600 MHz, acetone-d_6) δ 0.95 (3H, t, J = 7.2), 1.39 (2H, sext, J = 7.2), 1.93 (2H, quint, J = 7.2), 4.05 (3H, s), 4.36 (2H, t, J = 7.2), 7.72-7.73 (1H, m), 7.78-7.79 (1H, m), 9.11 (1H, s); ^{19}F NMR (565 MHz, acetone-d_6) δ 85.6 (3F, s); Water content: 415 ppm.

1-Butyl-3-methylimidazolium methyl sulfate ([bmim][MeSO₄])[67]


[bmim][MeSO₄]

Under argon atmosphere, a 1.0 equiv. amount of dimethyl sulfate (6.3 g) was added to a solution of 1-butylimidazole (6.2 g, 50 mmol) and dry toluene (10 mL) at 0 °C. The reaction mixture was stirred at room temperature for overnight. The upper layer (toluene layer) was removed by decantation, and residual under layer was washed with Et$_2$O (10 mL) three times. The obtained oil was dried *in vacuo*, and then it was passed through alumina column (neutral Al$_2$O$_3$ 150 g, eluent: dichloromethane). The obtained solution was concentrated under reduced pressure, and dried *in vacuo* (<100 Pa, 50 °C) to give [bmim][MeSO₄] (4.7 g, 37% yield): colorless liquid. ^{1}H NMR (600 MHz, CDCl$_3$) δ 0.95 (3H, t, J = 7.2), 1.35 (2H, sext, J = 7.2), 1.87 (2H, quint, J = 7.2), 3.72 (3H, s), 4.02 (3H, s), 4.25 (2H, t, J = 7.2), 7.45-7.46 (1H, m), 7.55-7.56 (1H, m), 9.44 (1H, s); Water content: 590 ppm.

1-Butyl-3-methylimidazolium dimethyl phosphate ([bmim][Me₂PO₄])[68]

[bmim][Me₂PO₄]

Under argon atmosphere, a 1.0 equiv. amount of trimethyl phosphate (4.2 g) was added to a solution of 1-butylimidazole (3.7 g, 30 mmol) and dry CH$_3$CN (6 mL). The reaction mixture was stirred at 80 °C for 7 days. The solvent was removed under reduced pressure, and dried *in vacuo*. The obtained oil was washed with Et$_2$O (10 mL) three times, and dried *in vacuo* again, and treated with activated carbon (granular, 3 g) in methanol (30 mL). The filtrate was concentrated under reduced pressure, and dried *in vacuo* (<100 Pa, 50 °C) to give [bmim][Me₂PO₄] (7.5 g, 95% yield): pale yellow liquid. ^{1}H NMR (600 MHz, CDCl$_3$) δ 0.96 (3H, t, J = 7.2), 1.37 (2H, sext, J = 7.2), 1.88 (2H, quint, J = 7.2), 3.60 (6H, d, J = 10.2), 4.06 (3H, s), 4.28 (2H, t, J = 7.2), 7.38-7.39 (1H, m), 7.53-7.54 (1H, m), 10.62 (1H, s); Water content: 3226 ppm.

Copper (II) bis(trifluoromethylsulfonyl)amide (Cu(Tf$_2$N)$_2$)[41]

$$CuO + 2Tf_2NH \xrightarrow{\ \ H_2O\ \ } Cu(Tf_2N)_2$$
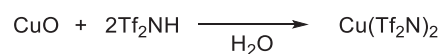
An aqueous solution of Tf$_2$NH (22.49 g in 50 mL of de-ionized water) was added to suspension of CuO (6.34 g, 80 mmol) in de-ionized water (50 mL) dropwise. The reaction mixture was stirred at 70 °C for 3 h and cooled to room temperature. The residual precipitate was removed by filtration using membrane filter (0.45 μm). The filtrate was concentrated under reduced pressure, and the obtained solid was dried *in vacuo* at 110 °C over 24 h to give desired product (24.70 g, quantitative yield).

Chapter 8. Measurement methods for physicochemical properties of ILs

8-1. Ionic conductivity

The ionic conductivities of IL (σ_i) were measured by the complex-impedance method using the following equation: $\sigma_i = J / R_{sol}$ [mS/cm] with an impedance analyzer (IM 3590, HIOKI E.E. Corp), where J is the cell constant (cm^{-1}) and R_{sol} is the resistance of the bulk IL at a high frequency limit. [1] A two-electrode cell (Pt-Pt electrodes) of a cell constant (1.27 cm^{-1}) was used, and the cell constant was determined with aqueous KCl solution purchased from Kanto Chemical Co., Inc. The cells were filled with IL samples in a nitrogen-filled glove box. While measuring, the cells were put in in a constant-temperature oven thermostatted at 30 °C. Frequencies were swept from 200 kHz to 20 Hz.
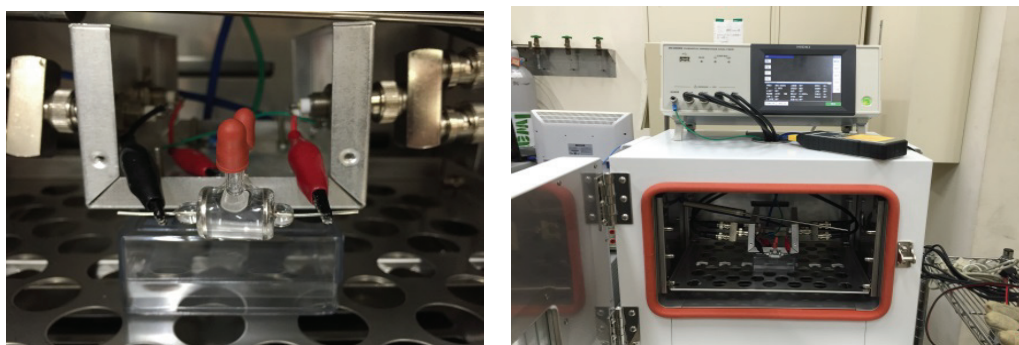
Figure 8-1. Equipment used for ionic conductivity measurements.

8-2. Viscosity

The viscosities of ILs were measured using the viscometer (DV2T, Brookfield Engineering Lab.) under argon atmosphere.

8-3. Solvatochromic parameters

The solvatochromic parameters β were measured by reported method[69] with the solvatochromic dyes, (2,6-dichloro-4-(2,4,6- triphenyl-1-pyridinio)phenolate (Reichardt's dye 33), 4-nitroaniline and *N,N*- diethyl-4-nitroaniline. The wavelength at the maximum absorption was recorded by UV/VIS spectrophotometer (V-550, JASCO Corp.).
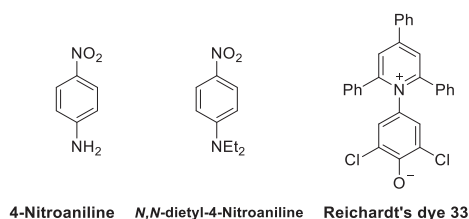

4-Nitroaniline   *N,N*-dietyl-4-Nitroaniline   Reichardt's dye 33

Figure 8-2. Dyes used for solvatochromic parameter measurements

Chapter 9. Physicochemical properties of ILs

The ** in the reference column means the measured value in this study.

Table 9-1. Physicochemical properties of ILs used in this paper (cation: [bmim] except for [emim][(HF)$_{2.3}$F])

Run	Name Cation	Name Anion	CAS No.	Formula weight [g/mol]	η (Viscosity) /25 °C [mPa·s]	Ref.	ρ (Density) /25 °C [g/cm³]	Ref.	Polarity E_T^N	α	β	π*	Ref.	σ /25 °C [mS/cm]	σ /30 °C [mS/cm]	Ref.
1	[bmim]	[Tf₂N]	174899-83-3	419.37	50.0	70	1.438	70	0.65	0.62	0.25	0.90	46	4.1	-	70
2	[bmim]	[FSA]	1235234-58-8	322.37	49.6	**	-		0.65	0.20	0.58	1.03	**	-	4.7	**
					33.1	**								-	8.8	**
3	[bmim]	[BF₄]	174501-65-6	229.05	113 /20 °C	71	1.202	7	0.66	0.63	0.38	1.05	46	3.6	4.5	7
					107.6	7										
4	[bmim]	[PF₆]	174501-64-5	284.19	261.0	72	1.368	73	0.67	0.63	0.19	1.04	46	1.5	2.5/35 °C	73
							1.370	74						1.6	2.1	72
5	[bmim]	[DCA]	448245-52-1	205.27	33 /20 °C	71	1.060	71	0.64	0.54	0.71	1.05	46	10.5	14.8/35 °C	73
							1.060	73						-	15.2	**
6	[bmim]	[TfO]	174899-66-2	288.28	75.3	75	1.300	76	0.67	0.63	0.46	1.00	46	2.9	4.4/35 °C	73
														-	3.7	**
7	[bmim]	[MeSO₄]	401788-98-5	250.31	213.2	77	1.211	76	0.64	0.53	0.66	1.06	46	-	2.2	78
8	[bmim]	[Me₂PO₄]	891772-94-4	264.26	651.4	**	1.162	79	-	0.51	1.00	1.06	69	-	0.6	**
9	[emim]	[(HF)₂.₃F]	841252-03-7	176.00	4.9	15	1.130	15	-	-	-	-	-	100	-	15

Table 9-2. Physicochemical properties of ILs used in this paper (anion: [Tf₂N])

Run	Cation	Anion	CAS No.	Formula weight [g/mol]	η (Viscosity) /25 °C [mPa·s]	Ref	ρ (Density) /25 °C [g/cm³]	Ref.	E_T^N	α	β	π^*	Ref.	σ /25 °C [mS/cm]	σ /30 °C [mS/cm]	Ref.
1	[emim]	[Tf₂N]	174899-82-2	394.33	33.0	60	1.517	80	0.69	0.66	0.28	0.90	46	9.2	10.7	7
					33.1	**	1.519	7						-	10.9	**
2	[bmim]	[Tf₂N]	174899-83-3	419.37	50.0	70	1.438	70	0.65	0.62	0.25	0.90	46	4.1	-	70
					49.6	**	-							-	4.7	**
3	[hmim]	[Tf₂N]	382150-50-7	447.42	67.0	81	1.378	82	0.65	0.65	0.25	0.98	46	2.3	-	83
					71.0	**	-							-	2.9	**
4	[omim]	[Tf₂N]	178631-04-4	475.47	92.5	84	1.321	84	0.63	0.60	0.28	0.97	46	1.4	-	83
					90.9	**	-							-	1.8	**
5	[bdmim]	[Tf₂N]	350493-08-2	433.38	93.3	70	1.416	70	0.55	0.38	0.24	1.01	46	2.1	-	70
					-	**	-							-	2.9	**
6	[MEmim]	[Tf₂N]	178631-01-1	421.33	44.9	**	1.500	85	0.66	0.62	0.23	1.00	**	-	-	**
														-	5.4	**
7	[bmtr]	[Tf₂N]	1231618-94-2	420.35	52.5	**	-		0.65	0.60	0.23	1.00	**	-	-	**
														-	3.4	**
8	[N₂₂₄]	[Tf₂N]	847452-51-1	424.42	120.0	55	1.380	55	0.60	0.55	0.26	0.95	**	1.6	-	55
														-	2.1	**
9	[PP₁₄]	[Tf₂N]	623580-02-9	439.45	182.0	55	1.379	55	0.55	0.50	0.36	0.92	46	1.1	-	55
														-	1.5	**
10	[Py₄]	[Tf₂N]	187863-42-9	416.36	59.0	86	1.450	86	0.59	0.48	0.12	1.01	46	3.2	-	86
							1.453	71						-	4.2	**

Chapter 10. References

1   H. Ohno, Ed., *Electrochemical Aspects of Ionic Liquids*, John Wiley & Sons, Inc., Hoboken, NJ, USA, 2011.

2   N. V Plechkova and K. R. Seddon, *Chem. Soc. Rev.*, 2008, **37**, 123–150.

3   J. P. Hallett and T. Welton, *Chem. Rev.*, 2011, **111**, 3508–3576.

4   M. Armand, F. Endres, D. R. MacFarlane, H. Ohno and B. Scrosati, *Nat. Mater.*, 2009, 8, 621–629.

5   S. I. Fletcher, F. B. Sillars, N. E. Hudson and P. J. Hall, *J. Chem. Eng. Data*, 2010, **55**, 778–782.

6   M. V Fedorov and A. a Kornyshev, *Chem. Rev.*, 2014, **114**, 2978–3036.

7   C. Schreiner, S. Zugmann, R. Hartl and H. J. Gores, *J. Chem. Eng. Data*, 2010, **55**, 1784–1788.

8   K. Matsumoto, Y. Okamoto, T. Nohira and R. Hagiwara, *J. Phys. Chem. C*, 2015, **119**, 7648–7655.

9   N. Wongittharom, C.-H. Wang, Y. Wang, C. Yang and J. Chang, *ACS Appl. Mater. Interfaces*, 2014, **6**, 17564–17570.

10   E. H. Cha, S. a. Lim, J. H. Park, D. W. Kim and D. R. Macfarlane, *J. Power Sources*, 2008, **178**, 779–782.

11   T. Sato, G. Masuda and K. Takagi, *Electrochim. Acta*, 2004, **49**, 3603–3611.

12   M. Wang, X. Xiao, X. Zhou, X. Li and Y. Lin, *Sol. Energy Mater. Sol. Cells*, 2007, **91**, 785–790.

13   I. W. Sun, H. P. Wang, H. Teng, S. G. Su, Y. C. Lin, C. W. Kuo, P. R. Chen and T. Y. Wu, *Int. J. Electrochem. Sci.*, 2012, **7**, 9765–9780.

14   P. Wasserscheid and T. Welton, Eds., *Ionic Liquids in Synthesis*, WILEY-VCH Verleg GmbH & Co. KGaA, Weinheim, Germany, 2003.

15   R. Hagiwara, K. Matsumoto, Y. Nakamori, T. Tsuda, Y. Ito, H. Matsumoto and K. Momota, *J. Electrochem. Soc.*, 2003, **150**, D195–D199.

16   R. Hagiwara, T. Hirashige, T. Tsuda and Y. Ito, *J. Fluor. Chem.*, 1999, **99**, 1–3.

17   T. Chang, K. Chang, T. Tsai, T. Chu and S. M. Sze, *Mater. Today*, 2016, **19**, 254–264.

18   R. Waser, R. Dittmann, C. Staikov and K. Szot, *Adv. Mater.*, 2009, **21**, 2632–2663.

19   C. Gopalan, Y. Ma, T. Gallo, J. Wang, E. Runnion, J. Saenz, F. Koushan, P. Blanchard and S. Hollmer, *Solid. State. Electron.*, 2011, **58**, 54–61.

20   Y. Nishi, *Curr. Appl. Phys.*, 2011, **11**, e101–e103.

21   W. Devulder, K. Opsomer, F. Seidel, A. Belmonte, R. Muller, B. De Schutter, H. Bender, W. Vandervorst, S. Van Elshocht, M. Jurczak, L. Goux and C. Detavernier, *ACS Appl. Mater. Interfaces*, 2013, **5**, 6984–6989.

22   M. Haemori, T. Nagata and T. Chikyow, *Appl. Phys. Express*, 2009, **2**, 061401.

23   T. Tsuruoka, K. Terabe, T. Hasegawa and M. Aono, *Nanotechnology*, 2010, **21**, 425205.

24   T. Hino, T. Hasegawa, K. Terabe, T. Tsuruoka, A. Nayak, T. Ohno and M. Aono, *Sci. Technol. Adv. Mater.*, 2011, **12**, 013003.

25   T. Tsuruoka, K. Terabe, T. Hasegawa, I. Valov, R. Waser and M. Aono, *Adv. Funct. Mater.*, 2012, **22**, 70–77.

26   S. Tappertzhofen, I. Valov, T. Tsuruoka, T. Hasegawa, R. Waser and M. Aono, *ACS Nano*, 2013, **7**, 6396–6402.

27   S. Haswgawa, K. Kinoshita, S. Tsuruta and S. Kishida, *ECS Trans.*, 2013, **50**, 61–67.

28   K. Kinoshita, *ECS Trans.*, 2015, **69**, 11–17.

29   J. A. Thornton, *Annu. Rev. Mater. Sci.*, 1977, **7**, 239–260.

30   K. R. Seddon, A. Stark and M.-J. Torres, *Pure Appl. Chem.*, 2000, **72**, 2275–2287.

31   M. Eikerling, A. A. Kornyshev and A. R. Kucernak, *Phys. Today*, 2006, **59**, 38–44.

32   N. Yaghini, L. Nordstierna and A. Martinelli, *Phys. Chem. Chem. Phys.*, 2014, **16**, 9266–9275.

33   H. Yuan, H. Shimotani, A. Tsukazaki, A. Ohtomo, M. Kawasaki and Y. Iwasa, *J. Am. Chem. Soc.*, 2010, **132**, 6672–6678.

34   F. Nardi, D. Ielmini, C. Cagli, S. Spiga, M. Fanciulli, L. Goux and D. J. Wouters, *Solid. State. Electron.*, 2011, **58**, 42–47.

35   K. Kinoshita, S. Tsuruta, S. Hasegawa, T. Fukuhara and S. Kishida, *MRS Proc.*, 2012, **1430**, 105–109.

36   S. Long, X. Lian, T. Ye, C. Cagli, L. Perniola, E. Miranda, M. Liu and J. Sune, *IEEE Electron Device Lett.*, 2013, **34**, 623–625.

37   K. Kinoshita, K. Tsunoda, Y. Sato, H. Noshiro, S. Yagaki, M. Aoki and Y. Sugiyama, *Appl. Phys. Lett.*, 2008, **93**, 033506.

38   S. P. Thermadam, S. K. Bhagat, T. L. Alford, Y. Sakaguchi, M. N. Kozicki and M. Mitkova, *Thin Solid Films*, 2010, **518**, 3293–3298.

39   J. Park, S. Jung, W. Lee, S. Kim, J. Shin, D. Lee, J. Woo and H. Hwang, *IEEE Electron Device Lett.*, 2012, **33**, 646–648.

40   F.-T. Chin, Y.-H. Lin, W.-L. Yang, C.-H. Liao, L.-M. Lin, Y.-P. Hsiao and T.-S. Chao, *Solid. State. Electron.*, 2015, **103**, 190–194.

41   K. Murase, K. Nitta, T. Hirato and Y. Awakura, *J. Appl. Electrochem.*, 2001, **31**, 1089–1094.

42   Y. Chao Yang, F. Pan and F. Zeng, *New J. Phys.*, 2010, **12**, 023008.

43   A. Chen, *Appl. Phys. Lett.*, 2010, **97**, 263505.

44   A. Harada, H. Yamaoka, R. Ogata, K. Watanabe, K. Kinoshita, S. Kishida, T. Nokami and T. Itoh, *J. Mater. Chem. C*, 2015, **3**, 6966–6969.

45   Y. Katayama, R. Fukui and T. Miura, *J. Electrochem. Soc.*, 2007, **154**, D534–D537.

46   P. G. Jessop, D. a. Jessop, D. Fu and L. Phan, *Green Chem.*, 2012, **14**, 1245–1259.

47   A. Harada, H. Yamaoka, K. Watanabe, K. Kinoshita, S. Kishida, Y. Fukaya, T. Nokami and T.

Itoh, *Chem. Lett.*, 2015, **44**, 1578–1580.

48   T. Katase, K. Murase, T. Hirato and Y. Awakura, *J. Appl. Electrochem.*, 2007, **37**, 339–344.

49   S. Jana, A. Parthiban and C. L. L. Chai, *Chem. Commun.*, 2010, **46**, 1488–1490.

50   C. C. Weber, A. F. Masters and T. Maschmeyer, *J. Phys. Chem. B*, 2012, **116**, 1858–1864.

51   H. Tokuda, K. Hayamizu, K. Ishii, M. A. B. H. Susan and M. Watanabe, *J. Phys. Chem. B*, 2005, **109**, 6103–6110.

52   K. Shimojo, N. Kamiya, F. Tani, H. Naganawa, Y. Naruta and M. Goto, *Anal. Chem.*, 2006, **78**, 7735–7742.

53   Y. Jeong and J. S. Ryu, *J. Org. Chem.*, 2010, **75**, 4183–4191.

54   R. Romeo, S. V. Giofrè, C. Carnovale, A. Campisi, R. Parenti, L. Bandini and M. A. Chiacchio, *Bioorg. Med. Chem.*, 2013, **21**, 7929–7937.

55   Z.-B. Zhou, H. Matsumoto and K. Tatsumi, *Chem. Eur. J.*, 2005, **11**, 752–766.

56   M. L. P. Le, F. Alloin, P. Strobel, J.-C. Leprêtre, C. Pérez del Valle and P. Judeinstein, *J. Phys. Chem. B*, 2010, **114**, 894–903.

57   Z.-B. Zhou, H. Matsumoto and K. Tatsumi, *Chem. Eur. J.*, 2006, **12**, 2196–2212.

58   L. L. Tolstikova and B. A. Shainyan, *Russ. J. Org. Chem.*, 2006, **42**, 1068–1074.

59   J. R. Harjani, R. D. Singer, M. T. Garcia and P. J. Scammells, *Green Chem.*, 2009, **11**, 83–90.

60   H. Matsumoto, H. Sakaebe, K. Tatsumi, M. Kikuta, E. Ishiko and M. Kono, *J. Power Sources*, 2006, **160**, 1308–1313.

61   Q. Zhang, K. Cai, Z. Jin, S. Wang and S. Sun, *J. Chem. Eng. Data*, 2010, **55**, 4044–4047.

62   D. Fang, J. Cheng, K. Gong, Q.-R. Shi, X.-L. Zhou and Z.-L. Liu, *J. Fluor. Chem.*, 2008, **129**, 108–111.

63   Y. Yoshida, K. Muroi, A. Otsuka, G. Saito, M. Takahashi and T. Yoko, *Inorg. Chem.*, 2004, **43**, 1458–1462.

64   N. Srivastava, M. Shukla and S. Saha, *Indian J. Chem. - Sect. A Inorganic, Phys. Theor. Anal. Chem.*, 2010, **49**, 757–761.

65   C. M. Sabaté and H. Delalu, *Eur. J. Inorg. Chem.*, 2012, **2012**, 866–877.

66   N. V. Ignat'ev, P. Barthen, A. Kucheryna, H. Willner and P. Sartori, *Molecules*, 2012, **17**, 5319–5338.

67   J. D. Holbrey, W. M. Reichert, R. P. Swatloski, G. A. Broker, W. R. Pitner, K. R. Seddon and R. D. Rogers, *Green Chem.*, 2002, **4**, 407–413.

68   A. Zicmanis and L. Anteina, *Tetrahedron Lett.*, 2014, **55**, 2027–2028.

69   Y. Fukaya, K. Hayashi, M. Wada and H. Ohno, *Green Chem.*, 2008, **10**, 44–46.

70   S. Katsuta, Y. Shiozawa, K. Imai, Y. Kudo and Y. Takeda, *J. Chem. Eng. Data*, 2010, **55**, 1588–1593.

71   R. Bini, M. Malvaldi, W. R. Pitner and C. Chiappe, *J. Phys. Org. Chem.*, 2008, **21**, 622–629.

72   W. Li, Z. Zhang, B. Han, S. Hu, Y. Xie and G. Yang, *J. Phys. Chem. B*, 2007, **111**, 6452–6456.

73   O. Zech, A. Stoppa, R. Buchner and W. Kunz, *J. Chem. Eng. Data*, 2010, **55**, 1774–1778.

74   S. Holopainen, M. Nousiainen, J. Puton, M. Sillanpää, U. Bardi and A. Tolstogouzov, *Talanta*, 2011, **83**, 907–915.

75   M. Ge, R. Zhao, Y. Yi, Q. Zhang and L. Wang, *J. Chem. Eng. Data*, 2008, **53**, 2408–2411.

76   M. Tariq, P. A. S. Forte, M. F. C. Gomes, J. N. C. Lopes and L. P. N. Rebelo, *J. Chem. Thermodyn.*, 2009, **41**, 790–798.

77   A. B. Pereiro, P. Verdía, E. Tojo and A. Rodríguez, *J. Chem. Eng. Data*, 2007, **52**, 377–380.

78   Y. H. Yu, A. N. Soriano and M. H. Li, *Thermochim. Acta*, 2009, **482**, 42–48.

79   Y. H. Gong, C. Shen, Y. Z. Lu, H. Meng and C. X. Li, *J. Chem. Eng. Data*, 2012, **57**, 33–39.

80   M. Geppert-Rybczyńska, A. Heintz, J. K. Lehmann and A. Golus, *J. Chem. Eng. Data*, 2010, **55**, 4114–4120.

81   T. Mandai, M. Imanari and K. Nishikawa, *Chem. Phys. Lett.*, 2011, **507**, 100–104.

82   S. S. Moganty and R. E. Baltus, *Ind. Eng. Chem. Res.*, 2010, **49**, 9370–9376.

83   K. Nakamura and T. Shikata, *ChemPhysChem*, 2010, **11**, 285–294.

84   A. E. Andreatta, A. Arce, E. Rodil and A. Soto, *J. Chem. Thermodyn.*, 2009, **41**, 1317–1323.

85   J. E. Bara, C. J. Gabriel, S. Lessmann, T. K. Carlisle, A. Finotello, D. L. Gin and R. D. Noble, *Ind. Eng. Chem. Res.*, 2007, **46**, 5380–5386.

86   H. Tokuda, K. Ishii, M. A. B. H. Susan, S. Tsuzuki, K. Hayamizu and M. Watanabe, *J. Phys. Chem. B*, 2006, **110**, 2833–2839.

Chapter 11. Publications

Report of results described in Chapter 3

A. Harada, H. Yamaoka, R. Ogata, K. Watanabe, K. Kinoshita, S. Kishida, T. Nokami and T. Itoh,

J. Mater. Chem. C, 2015, **3**, 6966–6969. (Inside front cover paper)
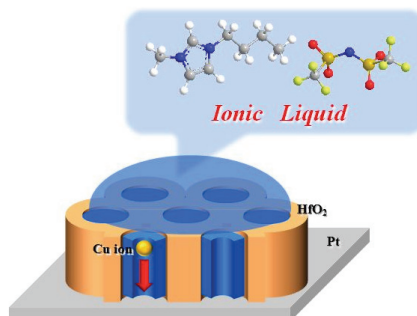
Report of results described in Chapter 4

A. Harada, H. Yamaoka, K. Watanabe, K. Kinoshita, S. Kishida, Y. Fukaya, T. Nokami and T. Itoh,

Chem. Lett., 2015, **44**, 1578–1580.
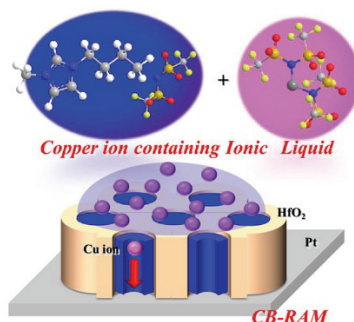
Report of results described in Chapter 5

A. Harada, H. Yamaoka, S. Tojo, K. Watanabe, A. Sakaguchi, K. Kinoshita, S. Kishida, Y. Fukaya, K. Matsumoto, R. Hagiwara, H. Sakaguchi, T.Nokami, and T. Itoh,

J. Mater. Chem. C, 2016, **4**, 7215-7222. (Back cover paper)
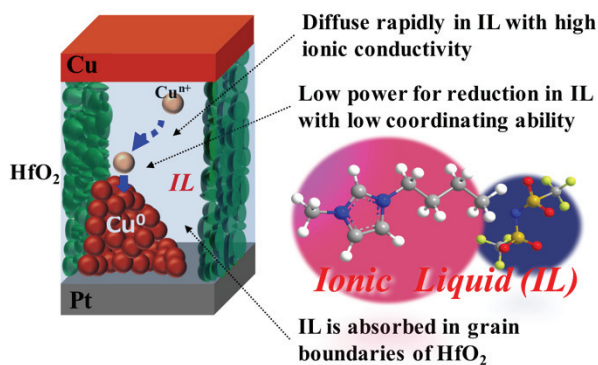
Journal of
Materials Chemistry C

Materials for optical, magnetic and electronic devices

www.rsc.org/MaterialsC
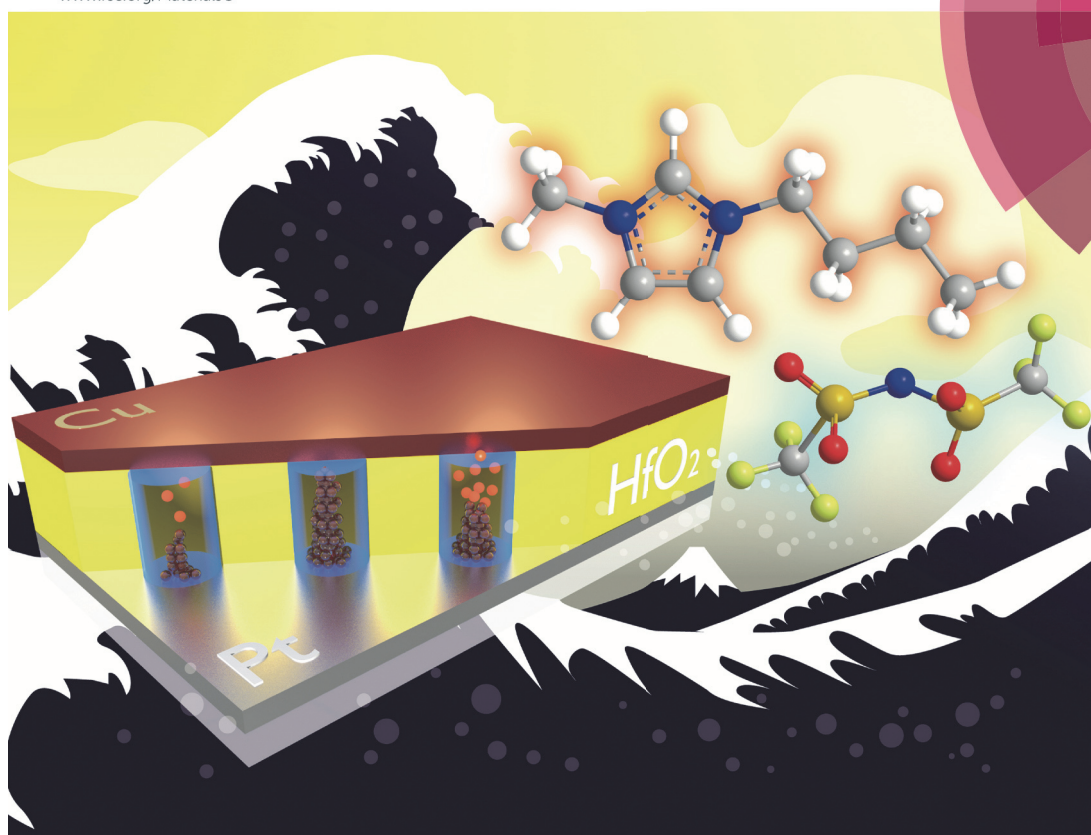
ROYAL SOCIETY OF CHEMISTRY

69
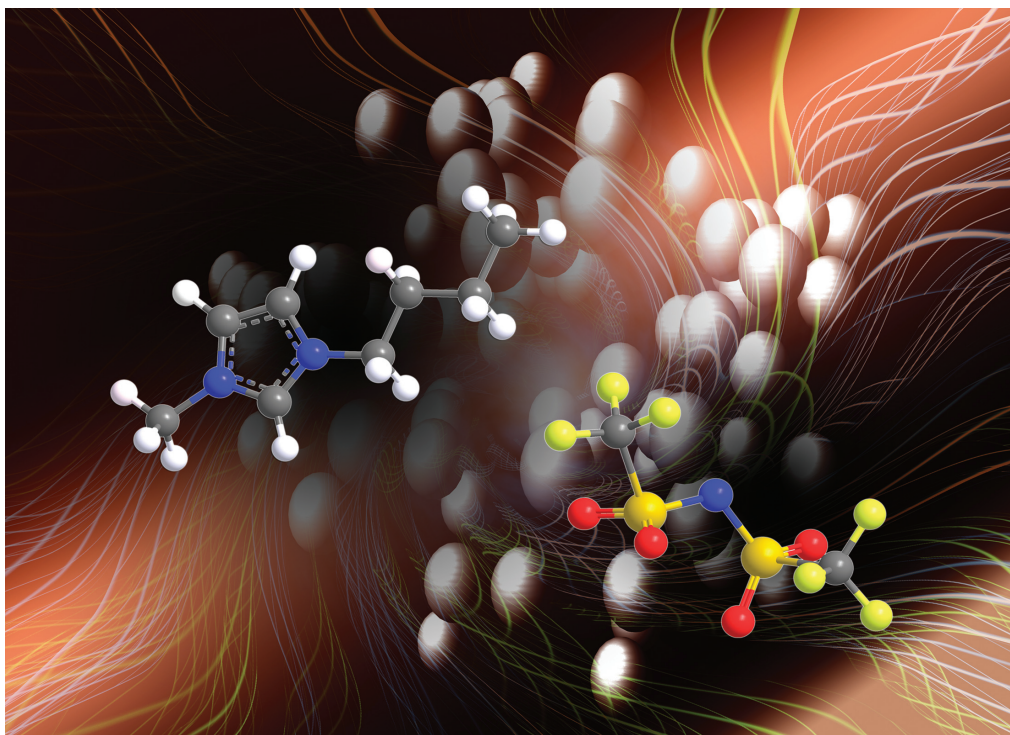
Showcasing research led by Professor Toshiyuki Itoh at Tottori University, Japan.

Improved performance of a conducting-bridge random access memory using ionic liquids

In this report, ionic liquids make it possible to provide high-performance CB-RAM that has low switching voltage and high cycling endurance.

As featured in:
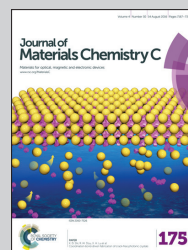
See K. Kinoshita, T. Itoh et al.,
J. Mater. Chem. C, 2016, 4, 7215.

ROYAL SOCIETY
OF CHEMISTRY

www.rsc.org/MaterialsC

Registered charity number: 207890

Acknowledgment

Akinori Harada

The Graduate School of Engineering

TOTTORI UNIVERSITY

July 2016